PHILOSOPHICAL TRANSACTIONS OF THE ROYAL SOCIETY A MATHEMATICAL, PHYSICAL & ENGINEERING SCIENCES

On the Dynamics of Near-Wall Turbulence

C. R. Smith, J. D. A. Walker, A. H. Haidari and U. Sobrun

Phil. Trans. R. Soc. Lond. A 1991 **336**, 131-175
doi: 10.1098/rsta.1991.0070

On the dynamics of near-wall turbulence

By C. R. Smith, J. D. A. Walker, A. H. Haidari and U. Sobrun

Department of Mechanical Engineering and Mechanics, Lehigh University, Bethlehem, Pennsylvania 18015, U.S.A.

A model of the dynamic physical processes that occur in the near-wall region of a turbulent flow at high Reynolds numbers is described. The hairpin vortex is postulated to be the basic flow structure of the turbulent boundary layer. It is argued that the central features of the near-wall flow can be explained in terms of how asymmetric hairpin vortices interact with the background shear flow, with each other, and with the surface layer near the wall. The physical process that leads to the regeneration of new hairpin vortices near the surface is described, as well as the processes of evolution of such vortices to larger-scale motions farther from the surface. The model is supported by recent important developments in the theory of unsteady surface-layer separation and a number of 'kernel' experiments which serve to elucidate the basic fluid mechanics phenomena believed to be relevant to the turbulent boundary layer. Explanations for the kinematical behaviour observed in direct numerical simulations of low Reynolds number boundary-layer and channel flows are given. An important aspect of the model is that it has been formulated to be consistent with accepted rational mechanics concepts that are known to provide a proper mathematical description of high Reynolds number flow.

1. Introduction

Turbulent flow near a surface is common in most fluid flow applications. Over the past 30 years, there has been intense interest in the basic physical processes near a wall that act to sustain the turbulent behaviour. In this paper, a model of wall turbulence will be presented which is based upon 15 years of complementary experimental, analytical and numerical studies of fully turbulent boundary layers, as well as 'kernel' flow problems. Here the term 'kernel' denotes a fundamental flow relevant to the dynamical processes in turbulent flows, but which nevertheless can be carefully studied in isolation, without the complications and competing influences that occur in a fully turbulent shear flow. The key element in the model is the hairpin vortex, initially proposed by Theodorsen (1952) and subsequently by others (see, for example, Willmarth & Tu 1967; Offen & Kline 1975; Perry & Chong 1982; Wallace 1982; Smith 1984; Robinson 1990; Smith *et al.* 1990; Walker 1990*a*). It will be argued that this flow structure is the basic building block of turbulence near a solid wall, and that the behaviour of the near-wall flow can be explained in terms of how such vortices interact with one another, the background shear flow, and the viscous flow near the surface. The symmetric hairpin vortex (see figure 1*a*) originally proposed by Theodorsen (1952) (see also Smith 1984; Acarlar & Smith 1987*a*, *b*) may be regarded as the simplest possible conceptual model which can account for the essential features of turbulent dynamics near the surface. Nevertheless, as a result of

Phil. Trans. R. Soc. Lond. A (1991) **336**, 131–175
Printed in Great Britain

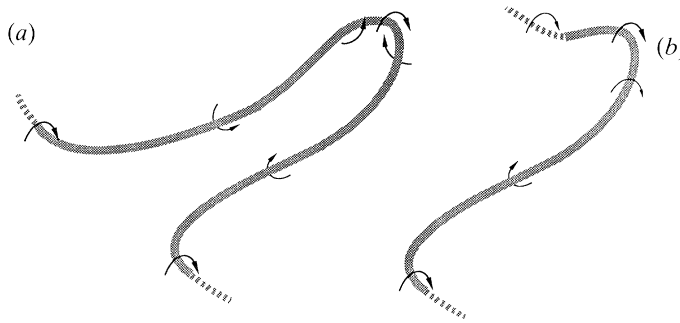

Figure 1. Schematic diagrams of typical hairpin vortex configurations, with sense of vorticity shown. Background flow is left to right. (*a*) Symmetric; (*b*) asymmetric.

the large number of competing vortices and background disturbances, the majority of the vortices in a turbulent boundary layer are expected to be asymmetric or 'one-legged' hairpins as shown in figure 1*b*. Recent syntheses (Kline & Robinson 1989; Robinson 1990, 1991) of the results of direct numerical simulations of low-Reynolds-number boundary-layer and channel flows confirm that this is the case. Robinson (1990) describes these 'one-legged' hairpins as 'quasi-streamwise vortices' (i.e. vortices that consist principally of a convected section of streamwise vorticity). Such vortices will be referred to as asymmetric vortices here, where it will be argued that the essential features of the interactions produced by symmetric hairpin vortices are the same for asymmetric hairpins.

The seminal experimental studies of Kline *et al.* (1967) on turbulent wall-layer structure inspired much experimental work (as well as subsequent direct numerical simulations of turbulence), some of which is discussed by Walker *et al.* (1989) and Robinson (1991). The general character of the readily observable features of the near-wall flow is well established at this stage, although an understanding of cause-and-effect relationships has proved elusive. There are two main aspects that dominate the near-wall flow, namely the 'low-speed streaks' and the 'bursting' phenomenon (Kline *et al.* 1967). For a given area of the wall, streaks may be readily observed during a majority of any observation period when a visualization medium, such as dye or hydrogen bubbles, is introduced into the flow near the surface. The streaks delineate regions where the cross-stream motion converges and the streamwise velocity is in deficit relative to the local mean velocity; sandwiched between the low-speed regions are zones of high-speed flow where the streamwise velocity exceeds the local mean. The low-speed streaks are typically separated by a distance of $100\nu/u_\tau$ (Kline *et al.* 1967; Smith & Metzler 1983), where ν is the kinematic viscosity and u_τ is the local mean friction velocity, and often extend in the streamwise direction a distance of up to $1000\nu/u_\tau$ (Blackwelder & Haritonidis 1983) (in other words an order of magnitude longer than the spanwise spacing).

The second predominant feature of the near-wall flow is the bursting event, a phenomenon that is observed at isolated streamwise and spanwise locations. The burst invariably initiates near a streak and culminates with an abrupt ejection of fluid from the near-wall region. This discrete ejection is quickly followed by a 'sweep' in which high-speed fluid from upstream undercuts the erupting fluid and the local streamwise velocity exceeds the mean velocity. It is evident that the bursting process involves a strong interaction with the surface flow; the nature and causes of this

interaction are a central theme of this paper. The eruptive processes that occur near the surface are of particular interest since they represent the fundamental means for regeneration and production of new turbulence. In addition, the subsequent ejection and concomitant sweeping action are the essential transport mechanisms for the elevated heat and mass transfer associated with turbulent surface flows. Furthermore, it is clear that rational methods of control and drag reduction must ultimately be based on the interruption of this cyclic behaviour near the surface.

It is common practice for the region below $y^+ = yu_\tau/\nu = 100$ to be denoted as the wall layer for both internal and external flows. The wall layer is often further subdivided into a sublayer, buffer region and a portion of the overlap (or logarithmic) region. Historically, this subdivision has been based on the shape of the mean profile rather than any dynamical features of the turbulence and is therefore somewhat artificial. This definition of the wall layer is also commonly used in descriptions of the kinematics of the low Reynolds number boundary layer with the zone above $y^+ = 100$ referred to as the 'outer region' (see, for example, the discussion by Robinson (1990)). Although this terminology is useful in defining fixed regions in space, it is constraining and potentially misleading to adopt classifications based on the mean profile when describing the fundamentally lagrangian dynamics of the near-wall flow. Consequently, broader definitions of the 'inner' and 'outer' regions of the flow near the surface are needed. In this paper, the 'outer' region of the boundary layer (or core region of an internal flow) refers to the portion of the flow field where the mechanisms of evolution and flow interactions are principally inviscid in character. The qualifier 'principally' is used here to allow inclusion, within this classification, of the physical processes that occur in vortex cores, where viscosity is important and generally acts to diffuse vorticity radially outward. Other physical situations falling into this category occur when detached shear layers develop at locations remote from the surface, or when vortex cores break and recombine upon close approach to one another (see, for example, Liu *et al*. 1985, 1986). In all of these situations, viscosity acts to diffuse zones of concentrated vorticity in very localized regions; however, the principal mechanisms of flow development and vortex evolution are still primarily inviscid in character. In the context of this definition, the outer region usually extends well below $y^+ = 100$ and, over some regions of the surface, may approach the wall rather closely at any instant in time (for example, during a 'sweep' event). The time-dependent wall layer or inner region is understood in this paper to denote the region close to the wall where the influence of viscosity is important. Sweep events create an inner region which is initially quite thin locally, but then subsequently thickens due to viscous diffusion. Thus, at any instant the imaginary surface in the flow denoting the approximate boundary between the inner viscous flow and the outer (effectively) inviscid region may be thought of as a highly contorted topology which approaches the wall closely in some regions and less so in others. It is well known that once the influence of the wall is removed, eruptive activity ceases (Uzkan & Reynolds 1967; Haidari & Smith 1988). In the turbulent wall layer, the no-slip condition is enforced through the influence of viscosity, and since this is a dominant effect, any explanation of bursting must directly address the role of viscosity in the process.

It is evident to even the casual observer of turbulent flow near a wall that vortices must play an important role in the dynamics of turbulence production. Kuchemann (1965) has described vortices as 'the sinews and muscles of fluid motion', and even the early conceptual models of boundary-layer turbulence were based on specific

PHILOSOPHICAL TRANSACTIONS OF THE ROYAL SOCIETY A MATHEMATICAL, PHYSICAL & ENGINEERING SCIENCES

types of vortex structures (see, for example, Theodorsen 1952; Black 1968; Willmarth & Tu 1967; Corino & Brodkey 1969). However, the turbulent boundary layer is a complex environment involving a highly sheared streamwise flow and a myriad of three-dimensional vortices which interact with the background shear flow, with each other, and with the viscous flow near the surface. In addition, such vortices are fundamentally lagrangian in character since they distort as they are convected downstream. Consequently, an experiment to establish cause-and-effect relationships for a moving vortex in a turbulent flow is extremely difficult, since it involves tracking a complex structure in an equally complex environment while trying to discern the influence of the vortex on its surroundings. Progress in understanding the dynamic processes of turbulent boundary layers has also been hampered by a lack of understanding of how vorticity evolves in a three-dimensional flow, as well as the general nature of the viscous response of a surface flow to the motion of a vortex above. Consequently, studies were initiated at Lehigh University in the late 1970s to answer the following fundamental questions: (1) what happens to the viscous flow near a solid surface at high Reynolds numbers when a vortex structure is convected above the surface; (2) what type of disturbance can provoke a wall-layer streak; and (3) how do three-dimensional vortices evolve in a background shear flow? The answers to these 'kernel' issues have been established through a combination of experimental and theoretical/numerical studies, where the objective was to examine a basic fluid mechanics phenomenon which has relevance to the dynamics of a turbulent boundary layer but within a well-controlled environment. By careful examination of these 'kernel' dynamics, it is possible to establish a fundamental basis for interpretation of observed events in the considerably more complicated surroundings of the turbulent boundary layer.

In recent years, there has been an increasing interest in the direct simulation of turbulence in channel flows (see, for example, Moin & Kim 1986) and boundary layers (Spalart 1988), wherein a small portion of a turbulent flow is simulated numerically, once various assumptions are made concerning spatial periodicity in the streamwise and cross-stream directions. Currently such simulations are restricted to relatively low Reynolds number and, although the computed mean statistics are found to agree with experimental data, it is clear that motions of relatively small spatial scale are not being resolved (see, for example, Zang 1991); consequently the numerical results cannot be considered grid-independent. It is often assumed that motions having small spatial scales are not important. However, in §5 it is argued that the important production events near the surface are predominantly narrow band eruptions that have very small streamwise and spanwise scales. Recently, Robinson (1990) has interrogated the direct simulation data for the low Reynolds number flat-plate boundary layer; he describes the kinematics of the observed coherent motions, most of which are associated with vortices (Robinson & Kline 1990). Many aspects of Robinson's (1990) conceptual kinematical model are consistent with the present model. Here, however, our central intent is to establish cause-and-effect relationships for the observed events near the surface and, thereby, establish the dynamics of the motion as opposed to a categorization of the kinematics. The areas where Robinson's work is consistent with the present model will be discussed subsequently. However, it is useful at the outset to mention some basic points of disagreement and to delineate some of the present objectives.

Robinson (1990), as well as many others, adopts the quadrant method to classify time-dependent motion in the turbulent boundary layer. This scheme, originally

PHILOSOPHICAL TRANSACTIONS OF THE ROYAL SOCIETY A MATHEMATICAL, PHYSICAL & ENGINEERING SCIENCES

introduced by Willmarth & Lu (1972) and Wallace *et al.* (1972), categorizes motions into one of four quadrants depending on the instantaneous sign of the fluctuating streamwise and normal velocities, u' and v', respectively. Within this classification, $(u'v')_4$ motions ($u' > 0, v' < 0$) are termed 'sweeps' and $(u'v')_2$ motions ($u' < 0, v' > 0$) are termed ejections. Because the quadrant approach defines an unambiguous criterion, and because it is associated with instantaneous contributions to the Reynolds stress, it is often used for the analysis and interpretation of direct numerical simulation data. However, for the purpose of establishing dynamics, we argue that simple quadrant analysis is potentially misleading; this is also true for other pointwise 'burst' detection schemes, such as the VITA technique of Blackwelder & Kaplan (1976) and other schemes which simply detect velocity excursions. Rather than ask which events contribute to the instantaneous Reynolds stress or generate local velocity excursions, it is more important to make a much sharper distinction by isolating those events which make lasting, unique and indelible contributions to $\overline{u'v'}$. It is worthwhile to mention two events which do not make such contributions. Consider first a transverse vortex which is advected to the right in either a uniform or a shear flow. It is relatively easy to establish (using, for example, a rectilinear vortex model (Milne-Thomson 1962)) that as the vortex passes an imaginary probe located either above or below the vortex core, contributions to $\overline{u'v'}$, as well as significant velocity excursions, will be recorded. However, if the vortex passes the probe on a horizontal trajectory, these $\overline{u'v'}$ contributions cancel and there is no net effect to the mean value; the velocity excursions are, of course, due to inviscid motion and have no direct relationship to turbulence production. It therefore seems inappropriate to assign the terminology 'sweeps' and 'ejections' to principally inviscid motions induced by a vortex (as in Robinson (1990) for example); note that although Robinson's (1990) definitions are unambiguous, we prefer the classical meaning of these terms wherein a discrete intermittent event is implied, as discussed by Corino & Brodkey (1969) (see also Blackwelder & Haritonidis 1983; Walker *et al.* 1989).

Secondly, consider the asymmetric hairpin vortex, or 'quasi-streamwise vortex' (Robinson 1990, 1991) shown in figure 1*b*. This terminology implies a vortex which has a significant portion of its vorticity oriented in the streamwise direction and generally at a shallow angle to the direction of the mean motion. Robinson (1990, 1991) concludes that the 'bursting process' is the result of a 'relatively long-lived, single, quasi-streamwise vortex which ejects low-speed fluid away from the wall by vortex induction'. In support of his model, Robinson (1990) argues that convected pieces of principally streamwise vorticity (cf. figure 1*b*) act as 'pumps' which produce 'ejections' and 'sweeps' as they move along. Again, however, if a vortex remains at nearly constant height above the wall, such instantaneous contributions to the Reynolds stress will not be permanent; they will be offset by contributions from a similar vortex that passes our imaginary probe at a subsequent time, but on a trajectory that is laterally displaced from that of the first vortex, so that the upflow zone of the first vortex is now in the downwash of the second vortex. Since the turbulent boundary layer must contain, on average, an equal number of positive and negative rotation sections of streamwise vortices in proximity to the surface, an equal number of such vortex-induced upflow and downflow events will occur over a large number of realizations. It thus appears that the dominant means of lasting Reynolds stress production cannot be explained through such kinematical arguments (Robinson 1990, 1991). Rather, we believe it is necessary to sharpen the focus

PHILOSOPHICAL TRANSACTIONS OF THE ROYAL SOCIETY A MATHEMATICAL, PHYSICAL & ENGINEERING SCIENCES

considerably and concentrate on those phenomena which produce unique contributions that are not subsequently offset by an essentially similar event. Close to the surface, there are at least two such unique evolutionary events, namely: (1) the eruptive production of new vorticity from the wall region, giving rise to new vortices (or vortical arches as described by Robinson (1990, 1991)), and (2) a subsequent inrush (or sweeping motion) toward the wall region following the eruptive events. At locations farther from the surface, local refocusing and rollup within the instantaneous vorticity field, as well as vertical motion of vortices (both up and down), appear to provide the physical means for lasting contributions to the Reynolds stress (Falco 1977, 1991).

2. The influence of vortex motion near a surface

To set the stage for subsequent discussion of the basic mechanisms of regeneration in turbulent boundary layers, the fundamental effect of vortex motion on the viscous flow near a solid surface will be described here. Over the past decade, the interactions of a wide variety of two- and three-dimensional vortex configurations with a surface flow have been studied (see, for example, Walker 1978; Doligalski & Walker 1978, 1984; Falco 1982; Ersoy & Walker 1985, 1987: Walker *et al.* 1987; Acarlar & Smith 1987*a*, *b*; Chu & Falco 1988; Chuang & Conlisk 1989; Smith *et al.* 1990; Taylor & Smith 1990; Haidari & Smith 1991; Greco & Smith 1991), including convected two-dimensional vortices, vortex rings and loops, and hairpin vortices near a wall. A general conclusion that emerges from these collective investigations is that a vortex in proximity to a surface will always provoke a discrete eruption of the viscous flow near the wall, provided that the vortex is sufficiently strong and/or close to the surface for a sufficient period of time. Moreover, the onset of this eruption is very abrupt and involves a sharply focused narrow-band outflow from the surface layer that culminates in the ejection of concentrated vorticity.

To appreciate the cause of this eruptive phenomenon, consider the schematic diagram in figure 2*a* of the essentially inviscid flow due to a vortex, and the corresponding velocity and pressure characteristics induced by the vortex near the surface as shown in figure 2*b*. The nature of the instantaneous flow pattern depends, in general, on the reference frame of the observer (see, for example, Doligalski & Walker 1984). However, a common basis for all situations corresponds to a reference frame which convects uniformly with the vortex core in the cross-vortex plane, which is defined in figure 2*c*. The normal plane to the vortex is perpendicular to the unit tangent $\hat{t}$ and contains both the normal and binormal to the vortex core. In general, the normal plane intersects the wall at some angle θ, which for most portions of a hairpin vortex will be close to $\frac{1}{2}\pi$. The cross-vortex plane is defined as the projection of normal plane on a plane normal to the wall as shown in figure 2*c*, with the normal and cross-vortex planes intersecting in a line parallel to the wall. The instantaneous streamline patterns shown in figure 2*a* may be considered to be representative of: (1) a transverse section of a hairpin, or (2) a portion of the leg of a hairpin vortex which is being convected in the streamwise direction, or (3) any portion of a three-dimensional vortex in motion at some oblique angle to the streamwise direction. For a three-dimensional vortex, the patterns in figure 2*b* may change somewhat at successive normal cross sections along the core, and axial motion along the vortex may give rise to spiraling motion near the core as indicated

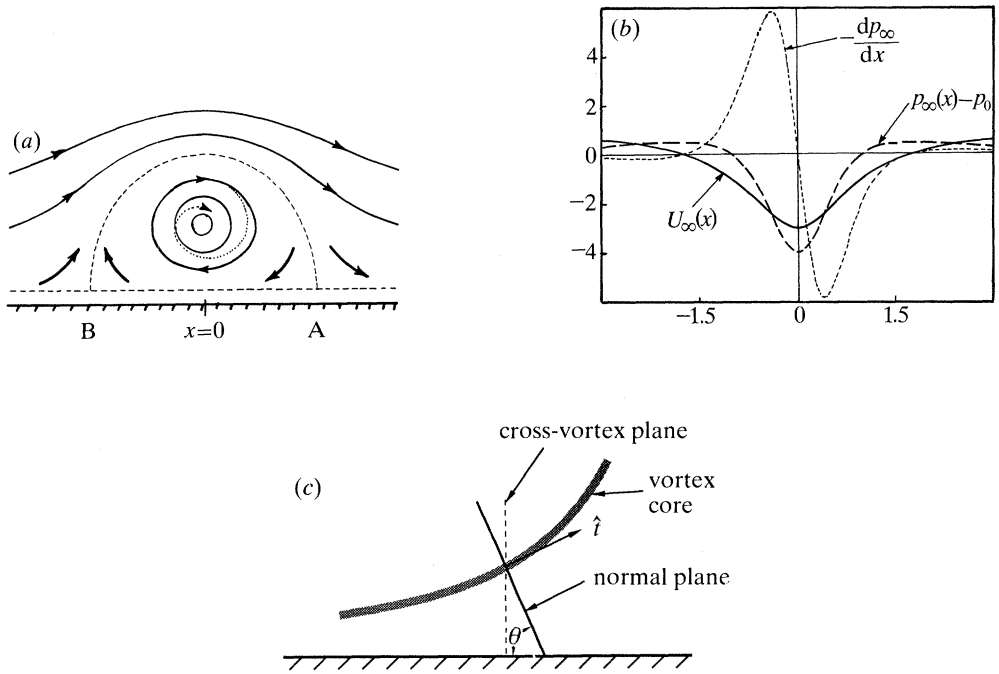

Figure 2. Instantaneous flow induced by a vortex near a wall in a frame of reference moving with the vortex core and in the cross-vortex plane: (*a*) instantaneous streamline patterns (..., possible spiral motion), (*b*) flow speed, pressure, and pressure gradient induced near the surface, (*c*) the cross-vortex plane.

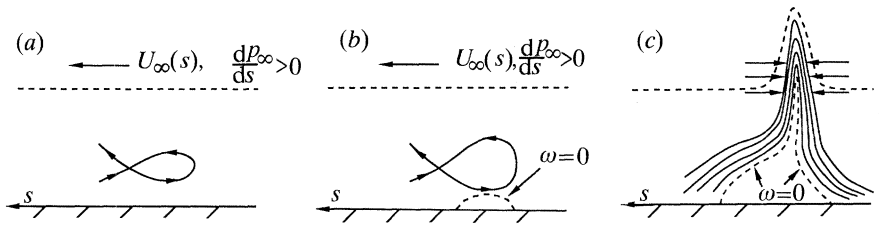

Figure 3. Schematic diagram of the stages in the separation of a two-dimensional surface layer (not to scale). (*a*) The evolution of recirculation near the surface. (*b*) Eddy growth. (*c*) Focusing and compression; —, equi-vorticity contours in the surface layer; →, compression of the erupting spike.

schematically by the dotted line in figure 2*a*. In addition, distortions in the symmetric patterns in figure 2*a* may arise due to neighbouring vortices. Nevertheless, the main characteristics of the flow pattern shown in figure 2 remain intact in most situations.

A variety of vorticity distributions within the vortex core are possible, but these do not alter the general features depicted in figure 2. One limit of vortex motion occurs when the vorticity is tightly concentrated in a small core, corresponding to a rectilinear vortex in two dimensions or a thin filament in three dimensions. In both situations, viscous effects are important only in the small region defining the core. In this case, realistic general solutions have been obtained that describe an axially decaying viscous core, wherein the vorticity diffuses slowly outward in the radial

direction (see, for example, Callegari & Ting 1978; Liu *et al.* 1986). Outside the core, the essentially inviscid motion sketched in figure 2*a* is produced.

The velocity field due to a rectilinear vortex may be determined analytically and is shown as an example in figure 2*a*, where the broken lines depict the Kelvin oval pattern with relative stagnation points at A and B to either side of the vortex centre. The broken line just above the wall in figure 2*a* is shown as a schematic indication that in any real fluid a viscous layer must exist to allow adjustment of the flow velocities to the no-slip condition at the surface. If the vortex core is located at a distance d from the wall, and x measures dimensionless distance (with respect to d) along the wall, the velocity and pressure distribution near the surface can be shown to be proportional to

$$U_\infty = 1-4/(x^2+1), \quad p_\infty(x)-p_0 = 4(x^2-1)/(x^2+1)^2, \tag{1}$$

respectively (Doligalski & Walker 1984), where p_0 is a constant. The stagnation points A and B are at $x = \pm\sqrt{3}$ respectively, where the pressure gradient $\mathrm{d}p_\infty/\mathrm{d}x$ vanishes and $p_\infty(x)$ achieves local maxima as shown in figure 2*b*. Directly under the vortex core at $x = 0$, the pressure reaches an absolute minimum and the induced flow speed near the surface attains an absolute maximum, with the motion near the surface being from right to left. Figure 2 shows that there are two regions of adverse pressure gradient (where the pressure increases in the local flow direction). The most significant zone of adverse pressure gradient is between the vortex centre at $x = 0$ and the outflow stagnation point at B; in this region the viscous flow near the surface 'sees' a rapidly decelerating external flow from right to left. Another adverse pressure gradient zone exists to the left of B, but here the rise in pressure toward B (and from the left) is much more gradual.

Although the distributions plotted in figure 2*b* pertain to a rectilinear vortex, qualitatively similar instantaneous flow patterns are to be expected in the cross-vortex plane, irrespective of the core vorticity distribution. For example, Batchelor (1967, p. 535) describes another possible limit of vortex motion in two dimensions where the vorticity is distributed over a finite area rather than being tightly concentrated in a small core; however, even in this situation there is virtually no difference in the tangential flow distribution near the wall (Doligalski & Walker 1984). A general conclusion that may be drawn from this discussion is that all vortices expose the flow near solid surfaces to a region of significant and persistent adverse pressure gradient between the centre of the core and the zone of outflow at B (cf. figure 2*b*).

To develop a rational theory of the processes that take place in the turbulent boundary layer at high Reynolds number, it is necessary to understand why and how local breakdowns and consequent eruptions of the near-wall flow occur. The initiation of such events will be referred to in this paper as unsteady separation phenomena, and the modern meaning of this terminology is as follows. Unsteady separation occurs in any situation where a viscous boundary layer, which has hitherto been passive and driven by the pressure distribution imposed by an outer inviscid flow, begins to interact strongly with the external flow for the first time in the process of separating from the surface. With motivation provided by the dissertation of Van Dommelen (1981), the general nature of such unsteady interactions has been appreciated only recently, as discussed by Cowley *et al.* (1990).

Two key elements are necessary to initiate a surface-layer separation or eruption. These are: (1) a persistent local adverse pressure gradient imposed near the surface

PHILOSOPHICAL TRANSACTIONS OF THE ROYAL SOCIETY A MATHEMATICAL, PHYSICAL & ENGINEERING SCIENCES

by the external flow, and (2) the influence of viscosity. Most recent studies of unsteady separation have been associated with two-dimensional flows. Although the repetitive separations of the turbulent wall-layer that comprise eruptive surface behaviour are three dimensional, the established sequence of events that occur in two-dimensional flows will be described here to motivate a subsequent discussion of the relevant three-dimensional turbulent processes. As shown in figure 3, let s denote a coordinate measuring distance along the surface from right to left in the local mainstream direction (taken arbitrarily from right to left to be consistent with figure 2), and let $U_\infty(s)$ and $p_\infty(s)$ be the flow speed and pressure just outside the viscous region near the surface. When the local pressure gradient imposed by the external flow is adverse (such as that induced by the vortex in figure 2*a* in the region between $x = 0$ and B), viscous effects quickly lead to the evolution of a zone of recirculation in the surface flow as indicated schematically in figure 3*a*. The appearance of a recirculating eddy (with a consequent line of zero vorticity) is a precursor of the surface-layer eruption that ultimately develops. It is therefore important to emphasize the role of viscosity as the catalyst for the entire process in conjunction with the local adverse pressure gradient. Different external pressure distributions can produce a wide variety of complex, unsteady flow topologies near the surface (see, for example, Doligalski & Walker 1984; Ersoy & Walker 1985, 1986), and in some circumstances the recirculation zone is attached to the surface (Van Dommelen & Shen 1980). If the external adverse pressure gradient is maintained, the recirculating eddy grows, as shown in figure 3*b*. However, the most significant characteristic of figure 3*a* and *b* is a persistent line of zero vorticity that has developed in the surface flow. The presence of this zero vorticity line is a central element of the modern theory of unsteady two-dimensional separation (Cowley *et al.* 1990). The MRS condition (Sears & Telionis 1975; Van Dommelen & Shen 1980; Cowley *et al.* 1990) requires that once the surface layer starts to erupt, the site of the strong outflows must develop somewhere along this zero vorticity line.

For the most part, numerical calculations of separating surface-layer flows have been attempted using conventional eulerian descriptions of the fluid motion with a numerical mesh that is fixed in space. The results of such computations have been controversial and of uncertain reliability once the separation process initiates (see, for example, the references discussed by Peridier & Walker (1989)). Only recently (Van Dommelen & Shen 1980; Peridier & Walker 1989) has it been possible to accurately compute the evolution of an erupting surface layer at high Reynolds number. Utilizing a lagrangian description of the fluid motion, wherein the trajectories of a large number of individual fluid particles are evaluated, accurate numerical solutions can be obtained, even when the boundary-layer flow focuses into a local narrow-band eruption (Cowley *et al.* 1990). As an example of this eruptive behaviour, consider the temporal development of the surface displacement thickness δ^* on a wall beneath the two-dimensional vortex shown in figure 4 (adapted from Peridier & Walker (1989); note that the specific situation considered by Peridier & Walker (1989) corresponds to a vortex having the opposite rotation to that shown in figure 2; the evolution depicted in figure 4 is therefore the mirror image of the results obtained by Peridier & Walker (1989)). Calculations were carried out by Peridier & Walker (1989) over a range of Reynolds numbers $Re = \kappa/\nu$, where κ is the vortex strength. The evolution shown in figure 4 is for $Re = 10^6$ and is a typical result for the range $5 \times 10^4 < Re < \infty$. Note that the boundary layer to the left of $x = 0$ (cf. figure 2) initially thickens faster than elsewhere, but not dramatically; this behaviour is due to a recirculating eddy

PHILOSOPHICAL TRANSACTIONS OF THE ROYAL SOCIETY A MATHEMATICAL, PHYSICAL & ENGINEERING SCIENCES

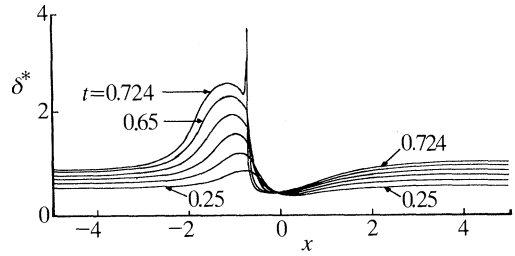

Figure 4. Temporal development of the displacement thickness induced in the surface boundary layer below the vortex shown in figure 2a; $Re = 10^6$ and $t = 0.25$ (0.10) 0.65.

which forms and then grows near the surface (Peridier *et al.* 1991*a*, *b*). It may be noted, however, that a sharp 'spike' develops abruptly in the displacement thickness near the end of the calculation, signifying the onset of a narrow-band surface-layer eruption. There are several significant problems in both the calculation and observation of such phenomena, which have been revealed by general theoretical descriptions of the process (Elliott *et al.* 1983; Smith 1988). First, the eruption develops over very short time scales (cf. figure 4) at locations which cannot be predicted *a priori*. For example, in the general configuration shown in figure 2a, an eruptive response of the surface layer can be expected to occur somewhere between $x = 0$ and B, but the precise location depends on the details of the specific external flow. It follows that such events are not easily anticipated in conventional numerical approaches, and it is difficult to make the timely local adjustments in either the spatial or temporal meshes that are necessary to adequately resolve such eruptions. Secondly, as the eruption initiates, the flow focuses into a band which is narrow in a direction tangential to the wall and which continues to narrow as the event develops, as indicated schematically in figure 3c. Within this narrow band, there are extreme variations in vorticity, with each side of the 'spike' consisting of a shear layer. In physical terms, a fluid particle on the zero vorticity line within the surface layer is compressed in the tangential direction to zero thickness (Cowley *et al.* 1990); by conservation of mass, this particle must elongate in the normal direction, which results in a local concentration of the surface-layer vorticity that moves rapidly away from the wall, as shown schematically in figure 3c. By this stage, the flow evolution is primarily inviscid (but nonlinear) in character and the subsequent development of the eruption becomes independent of the local external pressure gradient which initiated the entire process (Elliott *et al.* 1983). On the scale of the outer flow, the eruption appears as a sharp 'spike-like' ejection along a knife-edge containing elevated levels of vorticity. Furthermore, since the local flow 'forgets' the initiating pressure distribution, the theoretical account of Elliott *et al.* (1983) suggests that the 'spike' is a generic state ultimately reached by most erupting two-dimensional surface layers at high Reynolds numbers.

To date, accurate numerical solutions for erupting surface flows have been obtained using lagrangian methods for the impulsively moved circular cylinder (Van Dommelen & Shen 1980, 1982) and for vortex-induced separation (Peridier & Walker 1989; Peridier *et al.* 1991*a*, *b*), as well as a limited number of other physical situations (Cowley *et al.* 1990). These studies support the theoretical picture of Elliott *et al.* (1983) that erupting surface layers develop a generic structure at high Reynolds numbers, consisting of a sharp, 'spike-like', focused local outflow. The main

PHILOSOPHICAL TRANSACTIONS OF THE ROYAL SOCIETY A MATHEMATICAL, PHYSICAL & ENGINEERING SCIENCES

advantage of lagrangian methods is that when strong outflows occur, a large number of fluid particles are convected into such zones, which allow them to be well resolved; at present, lagrangian methods are the only means available to accurately compute such events at high Reynolds numbers. The onset of such 'spikes' has previously been noted in a variety of situations using conventional eulerian methods (see, for example, Walker 1978; Doligalski & Walker 1984; Ersoy & Walker 1986; Chuang & Conlisk 1988), but the phenomenon was not considered entirely credible until it was produced in its entirety using lagrangian methods. For vortex-induced motion near a wall (see Walker 1990*a* and the references therein), the development in the boundary layer may appear quite different up to the point of separation of the layer, depending on the precise nature of the external flow. However, the end result is that a narrow-band eruptive response occurs in all situations at high Reynolds numbers, once the surface flow has been exposed to the adverse pressure gradient due to a vortex for a sufficient period of time. An additional important conclusion is that as the circulation (or strength) of the vortex is increased and/or the vortex core is brought closer to the surface, the eruptive response occurs more rapidly.

Surface-layer eruptions have been observed in a number of experimental studies, involving aircraft trailing vortices and vortex rings (Harvey & Perry 1971; Cerra & Smith 1983; Walker *et al.* 1987; Chu & Falco 1988). In these studies the background environment was well-controlled, and although cause-and-effect relationships were clearly established, it was difficult to discern either the birth of separation events or the subsequent initial phase of the surface-layer eruption. The explanation is provided by the theoretical framework established by Van Dommelen & Shen (1982) and Elliott *et al.* (1983) which reveals that such events initiate at very small spatial scales and develop very abruptly. Because the eruption consists of a set of tightly focused shear layers that move rapidly away from the surface, and undoubtedly roll-up once free of the surface, the computation of such unsteady, strongly interactive flows at high Reynolds number is presently beyond the scope of modern computational methods. On the other hand, while theory and lagrangian calculations have established the physics of the initiation of the separation process, experiments clearly show that the process teminates with discrete portions of vorticity being ejected from the near-wall region (Harvey & Perry 1972; Cerra & Smith 1983; Chu & Falco 1988; Walker *et al.* 1987; Greco & Smith 1991). Consequently, during this regenerative process, new vorticity is introduced into the inviscid region away from the surface as a consequence of separation at the surface induced by a parent vortex.

An experimental example which clearly shows the focusing and eruption of the surface layer in the presence of controlled streamwise vortices is shown in figure 5 for vortex motion in an end-wall boundary layer. In the experimental configuration, a circular cylinder is mounted with its axis normal to a flat plate. As a subcritical laminar boundary layer approaches the cylinder junction, the Blasius boundary layer becomes unsteady, forming three-dimensional 'necklace' vortices periodically in the end-wall boundary layer upstream of the cylinder (Greco & Smith 1991). As shown schematically in figure 5*a*, these vortices engirdle the cylinder, with the outboard portions (the legs) moving periodically inward toward the cylinder wake as indicated in figure 5*b*. In figure 5*c–f*, the streamwise extensions of the necklace vortices are made visible through use of a hydrogen bubble wire located well off the surface and upstream of the cylinder. The hydrogen bubbles from the upstream wire are entrained into the vortices and are convected downstream, enabling visualization of the cores of the necklace vortices in a plane which is normal to the end-wall and

PHILOSOPHICAL TRANSACTIONS OF THE ROYAL SOCIETY A MATHEMATICAL, PHYSICAL & ENGINEERING SCIENCES

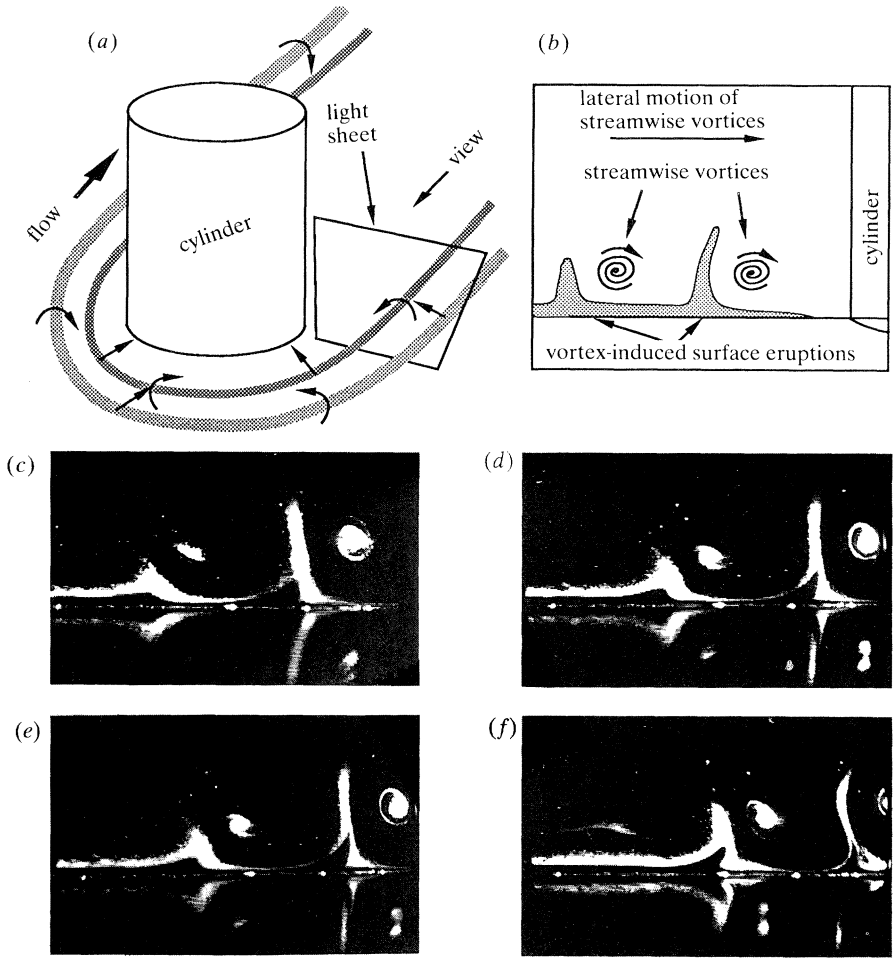

Figure 5. End-view of necklace vortex legs and induced surface eruptions. Visualization using hydrogen bubbles and light-sheet illumination. (*c*)–(*f*) A temporal sequence of end-view photographs illustrating streamwise necklace vortex legs and associated surface eruptions.

downstream of the cylinder. A second hydrogen bubble wire, located essentially on the surface, visualizes the response of the viscous flow near the surface to the motion of the vortices above. Note that the vortices evolve periodically and move progressively inboard toward the cylinder wake (from left to right in figure 5). Hence, the surface layer in the right portion of the photographs is exposed to the adverse pressure gradient due to a transient vortex for a relatively longer period of time than the surface layer to the left. Figure 5*c* shows that the vortex to the left has induced an upwelling from the surface layer similar to the early stages of development shown in figure 4. On the other hand, the more mature situation to the right in figure 5*c* shows how the surface flow has abruptly focused into the sharply eruptive spire that is predicted for the later stages of development shown in figure 4. Note how the temporal development of the eruptive spire in figure 5*c*–*f* illustrates a progressive focusing (or thinning) of the spire. Note also how the phenomenon develops in a frame of reference moving with the vortex, as predicted by theory (Peridier & Walker 1989; Peridier *et al.* 1991*a*, *b*).

PHILOSOPHICAL TRANSACTIONS OF THE ROYAL SOCIETY A MATHEMATICAL, PHYSICAL & ENGINEERING SCIENCES

In this section, a basic fluid mechanics phenomenon has been described wherein a vortex in proximity to a surface can provoke a narrow eruption of the viscous layer, resulting in the ejection of vorticity from the surface. Although much of the supporting work has been for two-dimensional flows, recent theories have addressed similar phenomena in three dimensions. These three-dimensional aspects will be taken up subsequently in §5, where the production process for turbulent boundary layers will be described.

3. Evolution of hairpin vortices

For turbulent flows near walls, Lighthill (1963, p. 96) has commented that the turbulence 'concentrates most of the vorticity much closer to the wall than before', (i.e. for a laminar boundary layer) 'although at the same time allowing some straggling vorticity to wander farther away from it'. As suggested in §1, the region near the surface is a complex environment dominated by the presence of a myriad of vortices which are believed to be predominantly of the hairpin type (Head & Bandyopadhyay 1981; Acarlar & Smith 1987*a*, *b*). (Falco (1991) suggests that structures similar to vortex rings ('typical eddies') are also present near the surface.) Such vortices constitute moving lagrangian disturbances which carry concentrated vorticity in the core region that diffuses progressively outward with time. These vortices are embedded in a highly sheared flow near the surface; over time they can be expected to distort into complex shapes, as well as to interact with one another, resulting in the evolution of complicated vorticity topologies. Consequently, since such flows require the tracking of multiple, complex, advecting regions of intense vorticity variations, they are enormously difficult to compute with reasonable accuracy at high Reynolds numbers using conventional eulerian numerical approaches. Viewed as a whole, the long-time evolution of the vorticity field above the wall is probably not deterministic in the usual sense and may be regarded as chaotic (Aubrey *et al.* 1988; Frisch & Orzag 1990). Nevertheless, it is clear that vortices are a dominant feature of the instantaneous flow, and furthermore, that some events associated with vortices are observed to occur repeatedly. Thus, although the prospects are not promising for the accurate calculation of the entire vorticity field in a boundary layer at high Reynolds numbers over long periods of time, it is possible to answer some fundamental 'kernel' questions that seek to establish cause-and-effect relationships for individual events of hypothesized relevance to wall turbulence. In particular, it is important to understand: (1) how hairpin vortices evolve and distort in a highly sheared environment, and (2) how such vortices interact with one another.

To understand the general features of three-dimensional vortex deformation in a shear flow, Hon & Walker (1987) have considered how a three-dimensional distortion develops on an otherwise two-dimensional line vortex advected in a uniform shear flow. Let $y > 0$ denote the upper half space containing a shear flow above a wall at $y = 0$; furthermore, let U_o denote the flow speed far from $y = 0$, and δ be a length characteristic of the thickness of the shear layer adjacent to the wall. We define dimensionless variables with respect to U_o and δ, and assume that a background unidirectional flow field given by $\boldsymbol{u} = U_b(y)\,\hat{\boldsymbol{i}}$ exists above the surface. (Note that the non-dimensional variables used here differ from those utilized by Hon & Walker (1987).) Here (x, y, z) measure distances in the streamwise, normal, and spanwise

directions, respectively, and $\hat{\boldsymbol{\imath}}$ is a unit vector in the x direction. The simplest representation of a shear flow near the surface is given by

$$U_{\mathrm{b}}(y) = \begin{cases} y, & y \leqslant 1, \\ 1, & y > 1, \end{cases} \tag{1}$$

corresponding to a uniform shear in the layer $0 \leqslant y < 1$. In addition, suppose that N vortex filaments are also present in the shear flow. The jth vortex has circulation Γ_j, is defined by the space curve C_j, and has position vector $\boldsymbol{X}_j(s,t)$, where t is non-dimensional time and s is a lagrangian coordinate measured along the vortex. For a collection of N thin vortex filaments advected in a background flow, an approximation to the Biot–Savart law gives (in dimensionless variables) the equation of motion for the jth vortex as:

$$\frac{\partial \boldsymbol{X}_j}{\partial t}(s,t) = \sum_{i=1}^{N} \epsilon_i \operatorname{sgn}(\Gamma_i) \int_{C_i} \frac{\partial \boldsymbol{X}_i}{\partial \xi} \wedge \frac{(\boldsymbol{X}_j - \boldsymbol{X}_i)}{\{|\boldsymbol{X}_j - \boldsymbol{X}_i|^2 + \mu^2 \delta_{ij}\}^{\frac{3}{2}}} \mathrm{d}\xi$$

$$- \sum_{i=1}^{N} \epsilon_i \operatorname{sgn}(\Gamma_i) \int_{\bar{C}_i} \frac{\partial \boldsymbol{X}_i}{\partial \xi} \wedge \frac{(\boldsymbol{X}_j - \boldsymbol{X}_i)}{|\boldsymbol{X}_j - \boldsymbol{X}_i|^3} \mathrm{d}\xi + U_{\mathrm{b}}(y)\,\hat{\boldsymbol{\imath}}, \tag{2}$$

where δ_{ij} is the Kronecker delta. Here $\bar{C}_i$ denotes the image vortex below the surface and

$$\epsilon_i = |\Gamma_i|/(4\pi U_{\mathrm{o}}\,\delta). \tag{3}$$

The parameters ϵ_i may be interpreted as the ratio of the vortex Reynolds number ($Re_{\mathrm{v}} = |\Gamma_i|/(4\pi\nu)$) to a local Reynolds number ($Re = U_{\mathrm{o}}\delta/\nu$) and are assumed small.

The vortex model utilized by Hon & Walker (1987) is due to Moore (1972), in which a small parameter μ, proportional to the vortex core radius a, is introduced in the denominator of the integrand in equation (2), to remove the singularity in the Biot–Savart integral. In order to define a particular vortex, the detailed distribution of the axial and swirl velocity in the vortex core must be prescribed at some initial instant, as well as some measure of the vortex core radius; the details of the vortex core flow directly influence the specific value of μ. To study vortex motion in proximity to a wall, it is desirable to work with thin filaments, which are characterized by relatively small values of a, to avoid situations where a thick-core vortex touches the wall prematurely, thus terminating the calculation. Note that careful numerical work is required for small values of a to ensure accurate determination of the vortex trajectories. Hon & Walker (1987) considered the evolution of a symmetric disturbance in a linear shear flow similar to that given by equation (1). A similar problem has also been considered by Hama (1962) and Aref & Flinchem (1984), who utilized a 'local induction' method to approximate the first integral in equation (1). Other vortex model equations may also be considered (Liu *et al.* 1985), but experience suggests (Sobrun 1991) that the qualitative evolution of a vortex filament is not crucially tied to the details of the treatment of the vortex core. Note that Aref & Flinchem (1984) have argued that a model equation of the form (2) is also consistent with the inviscid vorticity transport equation, provided that the core of the vortex is small and the time interval of interest is not large. Our principal objective here is to ascertain the general features of the shape of an evolving hairpin vortex over relatively short time periods. The studies cited above all show

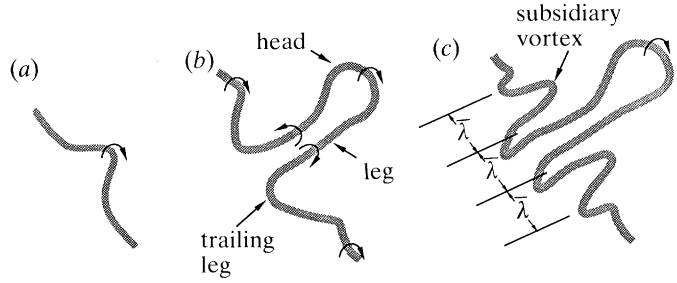

Figure 6. Evolution of a symmetric hairpin vortex in a shear flow. (*a*) Initial distortion, (*b*) development of vortex legs and head, (*c*) evolution of subsidiary vortices and penetration toward the surface.

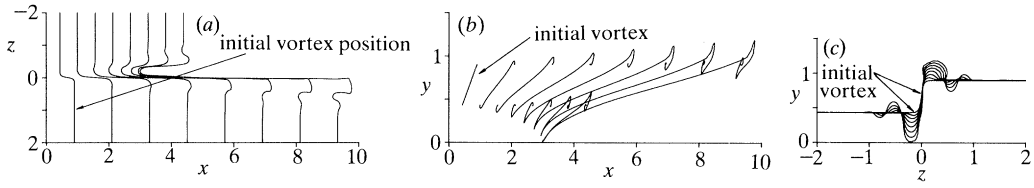

Figure 7. Evolution of a 'step' in a two-dimensional vortex convected in a uniform shear flow; the vortex position is shown every 40 time steps in (*a*) top view, (*b*) side view, and (*c*) end view.

that a generic pattern develops; some aspects of this are summarized schematically in figure 6.

The initial disturbance shown in figure 6*a* immediately starts to spread and grow in the streamwise direction, developing a shape which is independent of both the initial amplitude and orientation of the original disturbance. In figure 6, the vortex is convected from left to right and the sense of the vorticity is shown with arrows. Very rapidly a vortex head develops, rises from the wall, and bends back in the shear flow as shown in figure 6*b*; simultaneously, the trailing portions of the vortex legs move progressively downward toward the wall. As time increases, the vortex head moves farther from the wall while the legs move progressively closer to the surface. In addition, as shown in figure 6*c*, the original disturbance spreads laterally, producing similar configurations which Smith *et al.* (1990) refer to as subsidiary vortices. The development of the subsidiary vortices allows the original disturbance to multiply and spread in the spanwise direction through an interaction with the background shear flow. Note that the background shear is necessary to achieve the amplification in the streamwise direction shown in figure 6. Moreover, the characteristic spacing or spanwise separation distance $\bar{\lambda}$ of the vortex legs appears to be strongly dependent on the level of the background shear flow, with smaller $\bar{\lambda}$ spacings for increased shear rates (Hon & Walker 1987).

As previously suggested in §1, most vortices in the complex environment of the turbulent boundary layer are expected to be asymmetric rather than the ideal symmetric configuration depicted in figure 6. It is therefore important to understand the changes that asymmetric vortices introduce in the evolutionary picture shown in figure 6. Recently, Sobrun (1991) has carried out numerical integrations for a variety of asymmetric disturbances embedded in a uniform shear flow; results for a typical situation are shown in figure 7 where a vortex is embedded in the uniform shear flow described by equation (1). The initial vortex configuration has an asymmetric

PHILOSOPHICAL TRANSACTIONS OF THE ROYAL SOCIETY A MATHEMATICAL, PHYSICAL & ENGINEERING SCIENCES

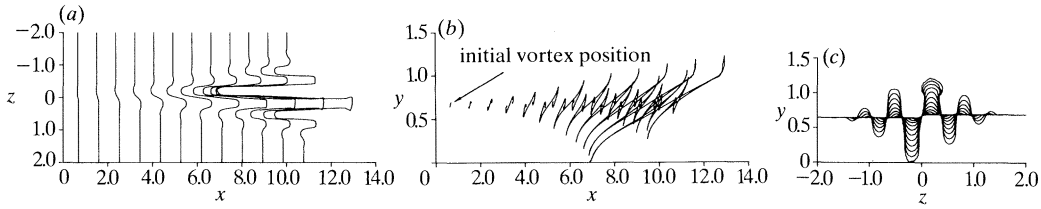

Figure 8. Evolution of a small 'step' in a two-dimensional vortex convected in a uniform shear flow: (*a*) top view, (*b*) side view, (*c*) end view; $\epsilon = 0.00267$, 440 time steps with $\Delta t = 0.034$. The vortex position is plotted every 40 time steps.

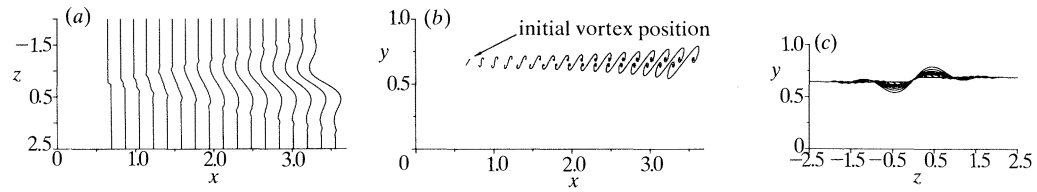

Figure 9. Evolution of an asymmetric hairpin for a reduced level of uniform shear: (*a*) top view, (*b*) side view, (*c*) end view; $\epsilon = 0.0134$, 640 time steps with $\Delta t = 0.0067$. The vortex position is plotted every 40 time steps.

distortion created by imposing a continuous 'step' in a two-dimensional line vortex as shown. The evolution of the vortex is described by equation (2) with $N = 1$. Calculations were carried out for $\epsilon = 0.00267$ using 280 time steps of $\Delta t = 0.034$; by this stage the evolutionary pattern of the vortex was established. It may be observed that a 'one-legged' hairpin vortex rapidly forms from the initial 'stepped vortex'. An asymmetric head develops and moves away from the surface (eventually rising into the uniform flow for $y > 1$), in much the same way as the symmetric case depicted in figure 6 (Hon & Walker 1987), with a trailing 'leg' portion developing and moving progressively towards the wall. Again the disturbance spreads laterally, producing subsidiary hairpins. From a broad examination of a number of other situations, Sobrun (1991) establishes that the pattern that forms is essentially independent of the initial asymmetric three-dimensional distortion in the vorticity field. As an example, consider the development shown in figure 8 where the 'step' in the initial two-dimensional vortex is very small. Again the characteristic pattern of figure 7 develops, but now to a somewhat more advanced state before the vortex core of the primary vortex leg touches the wall, thus terminating the computation.

The spanwise spacing $\bar{\lambda}$ of the transverse subsidiary lobes that form is dependent on the strength of the background shear flow. In figure 9, results are shown for a calculation with a five-fold increase in ϵ ($\epsilon = 0.0134$) and the same initial configuration as that for figure 8. It follows from equation (3) that, for a fixed vortex strength and shear layer thickness δ, larger values of ϵ correspond to a reduced magnitude of the background shear. Figure 9 illustrates that a pattern similar to figures 7 and 8 develops, but over a longer period of time and with increased spanwise spacing $\bar{\lambda}$ of the vortex lobes. Note that if a vortex with a spanwise distortion greater than the wavelength $\bar{\lambda}$ is introduced, 'one-legged' hairpin vortices will again form at all regions of high curvature. However, these initial hairpin vortices will then spread laterally in a manner similar to that shown in figures 7 and 8 until the spacing between lobes reaches a wavelength $\bar{\lambda}$ that is commensurate with the background shear flow (Sobrun 1991).

Most of the characteristics of the evolution of hairpin vortices discussed here have also been observed experimentally by Acarlar & Smith (1987*a*, *b*) and Haidari & Smith (1991), who created hairpin vortices artificially in a subcritical laminar boundary layer, observing the subsequent details of their behaviour and trajectories. The important aspects of the nonlinear and primarily inviscid interaction of hairpin vortices with a background shear flow can be summarized as follows:

1. As vortices are convected in a shear flow above a surface, any non-uniformity or region of relatively high local curvature in the vortex field will initiate the development of hairpin vortices, most of which will be asymmetric or one-legged hairpins.

2. During this development process, the vortex is progressively extended out over a larger relative streamwise distance; furthermore, an increasing portion of the vortex is transformed from transverse into streamwise vorticity with the formation and development of the vortex legs.

3. The relative spacing of the vortex legs $\bar{\lambda}$ is a function of the local strength of the background shear, decreasing with increasing shear.

4. The development of subsidiary hairpin vortices spreads the initial disturbance in the lateral direction.

5. The trailing legs of the hairpin vortex move progressively down toward the surface, which is a key aspect of the surface regeneration process to be discussed in §5.

Recently, Robinson (1990) has described the behaviour of vortices which appear in the low-Reynolds-number direct simulation results for a channel and a boundary-layer flow. Many of the kinematical features noted by Robinson (1990) can be explained in terms of the general behaviour shown in figures 7–9. For example, vortex 'arches' (referred to here as vortex heads) were observed to send legs toward the surface, similar to the process shown in figure 8. Another characteristic discussed by Robinson (1990) is that near the outer edge of the mean wall layer ($y^+ \approx 100$), typical local vortex topologies are observed to be either 'arches' (heads) or sections of streamwise vortices (legs). Generally, with increasing distance from the surface, the 'arches' are of a greater spanwise extent and the quasi-streamwise vortices are more broadly separated in spanwise extent (or equivalently are less populous). The evolution of hairpin vortices into much larger, but similar vortices in the outer part of the boundary layer has previously been observed or detected in a number of experiments (see, for example, Perry & Chong 1982; Smith & Lu 1990; Grass *et al.* 1991). To mimic this observation, Perry & Chong (1982) constructed a structural model of the turbulent boundary layer which consists of a hierarchy of hairpin vortices, with the smallest being near the surface and the largest farthest from the wall. Here two physical processes are discussed which offer a dynamical explanation of the observed behaviour.

As indicated in figures 7–9, asymmetric hairpin vortices may evolve from locations in the vorticity field where the vortex tubes congregate and exhibit relatively high local curvature. In addition, by an interactive process (to be described in §5), new vortices are generated intermittently near the surface. The characteristic spacing between vortex legs depends on the magnitude of the background shear; thus, near the surface (where the background shear is high) the spanwise spacing $\bar{\lambda}$ will be relatively small. Once a vortex head forms, it will migrate away from the surface via self-induction. As an individual vortex head and the upper legs migrate to regions of reduced shear in the boundary layer, the vortex heads will 'bloom' and the legs will

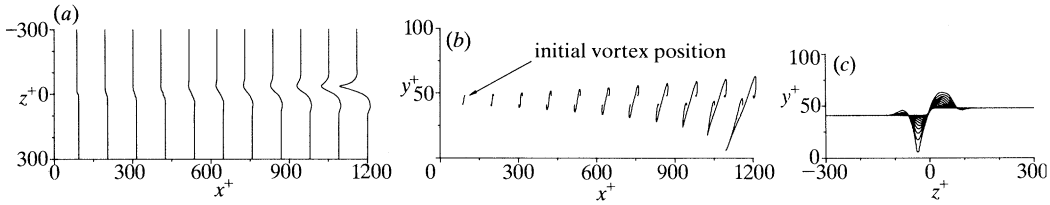

Figure 10. Evolution of an asymmetric hairpin vortex in a turbulent mean profile: (*a*) top view, (*b*) side view, (*c*) end view; $\epsilon = 0.0013$, 400 time steps with $\Delta t = 0.016$. The vortex position is plotted every 40 time steps.

spread farther apart. This phenomenon may be seen in figures 7*c* and 8*c* where the vortex head begins to broaden as it migrates out of the region of shear and into the uniform flow ($y > 1$).

To further illustrate this 'blooming' effect, calculations were carried out for an asymmetric hairpin vortex embedded in a shear flow characteristic of the mean profile of a flat plate turbulent boundary layer. For this simulation, we let y^+ and η denote scaled normal variables in the inner and outer parts of the boundary layer respectively, defined by

$$\eta = u_\tau y/\delta^*, \quad y^+ = (u_\tau Re)\, y, \tag{4}$$

where δ^* is the local displacement thickness, Re is the Reynolds number and u_τ is the dimensionless friction velocity (with respect to the local mainstream velocity). The mean wall-layer velocity profile function is denoted by $U^+(y^+)$ (see, for example, Bogucz & Walker 1988) and satisfies

$$U^+ = 0 \quad \text{at} \quad y^+ = 0; \quad U^+ \sim (1/\kappa) \ln y^+ + C_\mathrm{i} \quad \text{as} \quad y^+ \to \infty, \tag{5}$$

where $\kappa = 0.41$ is the Von Karman constant and $C_\mathrm{i} = 5.0$ is the inner region log–law constant. Also let $F'(\eta)$ denote the outer region defect function with

$$F'(\eta) \sim (1/\kappa) \ln \eta + C_\mathrm{o} \quad \text{as} \quad \eta \to 0; \quad F' \to 0 \quad \text{as} \quad \eta \to \infty, \tag{6}$$

where C_o is constant. A composite mean profile spanning the entire boundary layer is given by

$$U_\mathrm{b}(y) = 1 + u_\tau\{F'(\eta) + U^+(y^+) - (1/\kappa) \ln y^+ - C_\mathrm{i}\}. \tag{7}$$

Specific functions for $F'(\eta)$ and U^+ have been described by Bogucz & Walker (1988) and Walker *et al.* (1989). The skin friction is given in terms of the Reynolds number based on displacement thickness by

$$1/u_\tau = (1/\kappa) \ln Re_{\delta^*} + C_\mathrm{i} - C_\mathrm{o} \tag{8}$$

(see, for example, Bogucz & Walker 1988). Calculations were carried out for $Re_{\delta^*} = 2500$ ($u_\tau = 0.043$) with an asymmetric hairpin vortex, yielding the development shown in figure 10. The initial vortex configuration is the same as in figures 8 and 9 and the straight portions of the vortex in figure 10 are located near $y^+ = 40$. It may be seen that a hairpin head forms and then expands as it moves away from the wall. This broadening with increasing distance from the wall across a region of diminishing shear gives the appearance of fewer 'streamwise' vortices as well as wider 'arches' (or heads). Note that the lateral extent of the vortex head is comparable to the observed mean streak spacing for turbulent boundary layers of 100 wall layer units. In figure 11, the evolution is shown for the same configuration as used in figure 10, with ϵ doubled to $\epsilon = 0.025$. For the turbulent mean profile, the

PHILOSOPHICAL TRANSACTIONS OF THE ROYAL SOCIETY A MATHEMATICAL, PHYSICAL & ENGINEERING SCIENCES

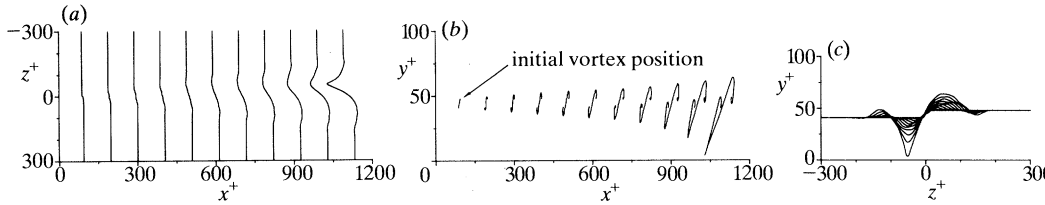

Figure 11. Evolution of an asymmetric hairpin vortex in a turbulent mean profile: (*a*) top view, (*b*) side view, (*c*) end view; $\epsilon = 0.0025$, 380 time steps with $\Delta t = 0.016$. The vortex position is plotted every 38 time steps.

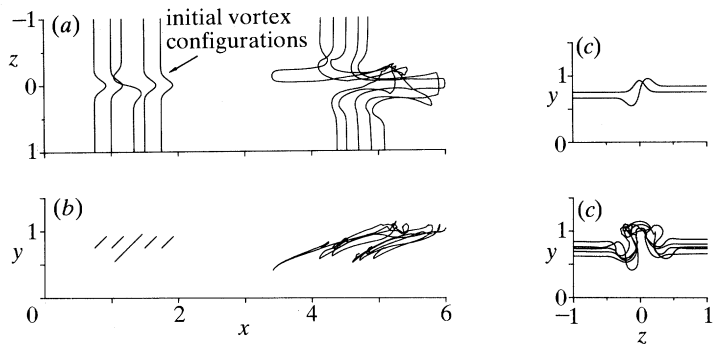

Figure 12. Evolution of multiple hairpin vortices in a uniform shear: (*a*) top view, (*b*) side view, (*c*) end view; all three coordinates are plotted on the same scale.

value of U_o may be considered fixed; thus, it follows from equation (3) that a larger value of ϵ corresponds to a stronger vortex. Upon comparison of figures 10 and 11, it is evident that the lateral rate of expansion of the vortex is much greater for the larger value of ϵ, with the head becoming almost twice as wide.

Of course the evolution of each individual vortex will not take place in isolation of the other vortices in the shear flow, and a second physical process, that of coalescence of smaller vortices to yield larger structures is also believed to occur. Indeed, recent experimental studies of passive surface vortex generators carried out by Gretta (1990) indicate that the outward migration of 'turbulent' hairpin vortices, introduced in an otherwise laminar boundary layer, occurs via a complex process of three-dimensional vortex pairing and amalgamation. This process results in both a rapid outward migration of the composite hairpin structures and a significant evolution into structures of larger scale. The study (Gretta 1990) further determined that the growth of scales by vortex amalgamation is also associated with the development of a logarithmic mean velocity profile as the flow evolves downstream.

The hypothesized physical process leading to hairpin amalgamation in a turbulent boundary layer can be described as follows. Near the surface (but within the outer inviscid region) the flow field contains a myriad of convected hairpin vortices of relatively small spanwise extent (typically on the order of $\Delta z^+ \approx 100$). As such vortices migrate upward out of the tangle of vorticity nearer the surface, they will expand laterally, but also will tend to intertwine and reinforce one another upon close approach. This process may be thought of as three-dimensional vortex pairing, and generally such vortex interactions tend to produce asymmetric hairpin vortices of somewhat larger scale than the original vortices. In figure 12, the results of a calculation for five vortices above a wall in a linear shear flow (cf. equation (1)) are

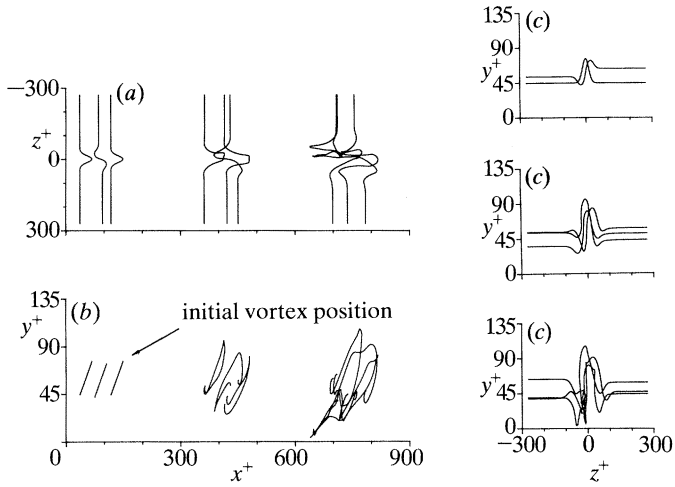

Figure 13. Evolution of three vortices in a turbulent mean profile: (*a*) top view, (*b*) side view, (*c*) end view; $\epsilon = 0.0013$, vortices shown after 120 and 240 time steps with $\Delta t = 0.016$.

shown. In equation (2), $N = 5$ and all the vortices have the same strength with $\epsilon = 0.002$. In the initial vortex configuration, four small symmetric hairpin vortices, that are aligned in the streamwise direction as shown, bracket a fifth asymmetric vortex. The vortices are shown after 160 time steps of $\Delta t = 0.025$ at a subsequent position downstream; observe that all five have intertwined over the three-dimensional extent of the vortices to produce what effectively appears as a single asymmetric hairpin vortex of somewhat larger spanwise extent (near the head). It is interesting to note how similar these hairpin agglomerations appear to some of the vortex-line tracings of Moin & Kim (1986) and Kim *et al.* (1987) from their low Reynolds number channel flow simulations, as well as to the recent measurements of Grass *et al.* (1991). Other calculations carried out by Sobrun (1991) suggest that the tendency for such interactions is high, producing expansive amalgamations of the vortex heads farther from the surface. An additional observation is that in this highly sheared environment, a small degree of asymmetry of the interacting vortices invariably leads to a greater degree of asymmetry in the product structures (cf. figure 12). Thus it is not surprising that only a small percentage of symmetric hairpin vortices are observed in the direct simulations (Robinson 1990). Similar intertwining behaviour is shown for the evolution shown in figure 13, where three vortices interact within a shear flow simulating a turbulent mean profile. Note the intertwining and the apparent amalgamation near the vortex heads, which produces an asymmetric vortex of somewhat larger scale. At the same time, individual vortex legs move rapidly down toward the surface.

One further point should be noted in relation to the evolution depicted in figures 12 and 13. Numerical solutions of the system described by equation (2) cannot be continued in time once two or more sections of a vortex move into close enough proximity such that the cores nearly touch. In principle, the calculation can be advanced in time in such situations by introducing a local computational zone in the region where the vortex cores are about to touch, and then solving the full Navier–Stokes equations within this local domain. Computations of this nature have been carried out by Liu *et al.* (1986), which suggest that the vortex cores within the

PHILOSOPHICAL TRANSACTIONS OF THE ROYAL SOCIETY A MATHEMATICAL, PHYSICAL & ENGINEERING SCIENCES

zone of close approach break and then rapidly reconnect to form new vortex topologies. The calculations shown in figures 12 and 13 terminate when a close approach of the individual vortices occurs near the vortex heads. This same mode of breakdown was invariably found to occur in a variety of other vortex configurations (Sobrun 1991), with the individual vortex heads always seeming to pile one upon another. This tendency suggests another possible mode of migration of vorticity from the wall region. A plausible next stage in the evolution depicted in figure 12 is for the vortices to break locally and recombine to form a closed vortex loop, which is then liberated to move farther away from the surface. Closed vortex rings (or loops) have sometimes been proposed as a basic vortex element of boundary layer turbulence. In particular, Falco (1991) argues that the large-scale motions in the outer part of the boundary layer consist mainly of recirculating vortex loops ('typical eddies'), which he regards as the main contributors to the Reynolds stress at locations remote from the surface. In this paper our main interest is in the processes very close to the surface, where we believe the main structure is the hairpin vortex. On the other hand, the physical origin of 'typical eddies' has been unclear and their existence has been controversial; the present computations suggest a possible process for such ring-vortex formation.

The following inviscid processes have been described here: (*a*) vortex expansion in regions of decreasing shear, (*b*) vortex coalescence to larger vortices, and (*c*) vortex reconnection to form loop vortices. These all contribute to both migration of vorticity away from the surface and growth into larger vortex structures. Indeed, it appears probable that the large overturning motions that are observed to encompass the entire boundary layer are composed of agglomerations of elementary vortices that originated adjacent to the surface (see also the structural model described by Falco (1991)).

Returning now to the region near the wall, it is evident from figures 10, 11, and 13 that the behaviour of the hairpin vortex legs is quite different than the vortex heads. As the legs penetrate toward the surface, the spacing between the legs diminishes as regions of increased shear are reached. Note also that the leg on the relatively stronger vortex shown in figure 11 reaches the vicinity of the wall somewhat faster than the vortex shown in figure 10 (see also Sobrun 1991). Near the surface there are many vortices which are subject to competing effects. Individual hairpin vortices which approach each other closely will tend to intertwine, but at the same time each vortex tries to send legs downward toward the surface. The combination of the large number of vortices and the narrowing of the distance between the legs thus gives the impression of an increased number of streamwise vortices nearer the surface (cf. Robinson 1990). It is expected that the legs of relatively weak hairpin vortices will dissipate as they penetrate the inner viscous region near the surface. On the other hand, relatively strong hairpin vortices can be expected to provoke a viscous–inviscid interaction with the near-wall flow via a regenerative process that is described in §5.

4. Low-speed streaks

A predominant feature of near-wall turbulent flow is the persistence of low-speed streaks having a typical scaled spacing of $\lambda^+ = \lambda u_\tau/\nu \approx 100$ over a range of Reynolds numbers (Smith & Metzler 1983). We now consider the origin of these streaks, their relationship to the vortex motion above, and the nature of their role in the dynamics of the near-wall flow. Because bursting is generally observed to initiate near a low-

PHILOSOPHICAL TRANSACTIONS OF THE ROYAL SOCIETY A MATHEMATICAL, PHYSICAL & ENGINEERING SCIENCES

speed streak, it has long been believed that streaks are a key aspect of the bursting process. Furthermore, because the streamwise extent of the streaks is often an order of magnitude greater than their average spanwise separation distance, the simplest conceptual model is that the streaks are caused by long counter-rotating vortices, aligned in the streamwise direction (see, for example, Blackwelder & Eckelmann 1979; Hatziavramidis & Hanratty 1979; Aubrey *et al.* 1988; Walker & Herzog 1989). Although this type of model does capture some important aspects of the near-wall flow, neither experiments nor the low-Reynolds-number direct numerical simulations (Moin & Kim 1986; Robinson 1990, 1991) support the concept of long counter-rotating vortex pairs embedded within the instantaneous wall-layer flow. Thus it is necessary to seek a more appropriate causal mechanism.

A point to be emphasized is that the existence of a relatively well-ordered pattern of low-speed streaks near the surface, existing beneath a much more complex outer flow, has profound implications for both the dynamics of the wall layer and the development of a rational theory to explain the processes involved. Descriptors such as 'relative inactivity' or 'quiescent period' have often been used to describe the near-wall motion over sections of the surface where low-speed streaks are present and relatively stable. The near-wall flow has also been described as exhibiting the 'footprints' of the outer motion during such periods (see, for example, the review by Willmarth 1975). Implicit in these descriptions is the rational mechanics concept of an unsteady outer flow which induces a pressure distribution near the surface, that in turn drives the evolution of the inner flow (at least temporarily).

Recently, Walker (1990*a*) considered a general wall-layer flow having a normal length scale $O(\nu/u_\tau)$ and containing streaks with a characteristic spanwise spacing of λ (with λ^+ large ($\lambda^+ \approx 100$)); it was demonstrated that the equations governing the near-wall motion are of the boundary-layer type in the limit of large Reynolds number. In other words, during the quiescent state the viscous wall layer near the surface remains thin and attached. In this phase of the motion, the unsteady vortex motion above this layer impresses a local pressure distribution across the thin wall layer, which drives the development of the inner viscous flow. Thus, the local wall layer development is principally described by the streamwise and cross-stream momentum boundary-layer equations (Walker 1990*a*). A subsequent event, in which the inner viscous region and outer region interact strongly, is referred to here as a viscous–inviscid interaction; this type of event is distinct from the quiescent state, since normal pressure gradients now become significant near the surface. Such interactions may be viewed as local breakdowns of the near-wall flow and are the special events which lead to the discrete injections of new vorticity from the wall into the outer portions of the boundary layer. The issue of how interactions of this nature develop will subsequently be addressed in §5. Here our object is to address what role, if any, the low-speed streaks play in the process.

The origin of the wall-layer streaks can be explained on the basis of a number of fundamental 'kernel' experiments (Acarlar & Smith 1987*a*, *b*; Taylor & Smith 1990; Haidari & Smith 1991) and numerical studies (Hon & Walker 1987). In the experimental studies, controlled hairpin vortices were created in an otherwise laminar boundary layer by a process of fluid injection at the wall; the lagrangian influence of such vortices on the near-wall flow was examined downstream. A schematic of the hairpin generation test section is shown in figure 14. Fluid is injected at the surface through a narrow, streamwise slot by using controlled injection of limited extent. The injected fluid interacts with the Blasius boundary layer to form

PHILOSOPHICAL TRANSACTIONS OF THE ROYAL SOCIETY A MATHEMATICAL, PHYSICAL & ENGINEERING SCIENCES

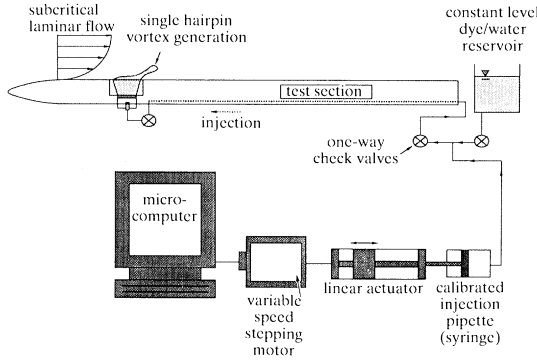

Figure 14. Experimental system for generating single hairpin vortices using controlled injection through a narrow streamwise slot into a subcritical laminar boundary layer.

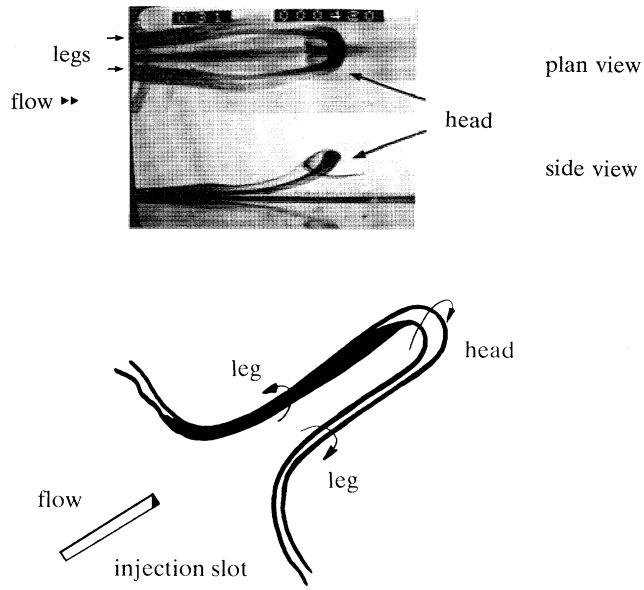

Figure 15. Illustration of experimental generation of a single hairpin vortex by surface injection using system shown in figure 14. (*a*) Dual-view picture of dye-marked single hairpin vortex. (*b*) Isometric schematic of single hairpin after generation.

an unstable shear layer which rolls up to form a single hairpin vortex. Figure 15 illustrates an example of a dual-view dye visualization of such a vortex; note that the vortex is well defined and symmetric. The development of the generated hairpin is then observed as it advects downstream.

The effect that the single hairpin vortex has on the surface layer was visualized using a transverse hydrogen bubble wire to generate a sheet of bubbles very near and parallel to the surface, as shown schematically in figure 16. In all situations, it was observed that the passage of the hairpin vortices produces low-speed streaks near the surface. This is illustrated in figure 17, taken from Haidari & Smith (1991), which shows plan-view hydrogen bubble visualization patterns created by the passage of a developing hairpin vortex at progressively increasing downstream distances. In figure 17*a–d*, the hydrogen bubble wire is located relatively far from the surface, and

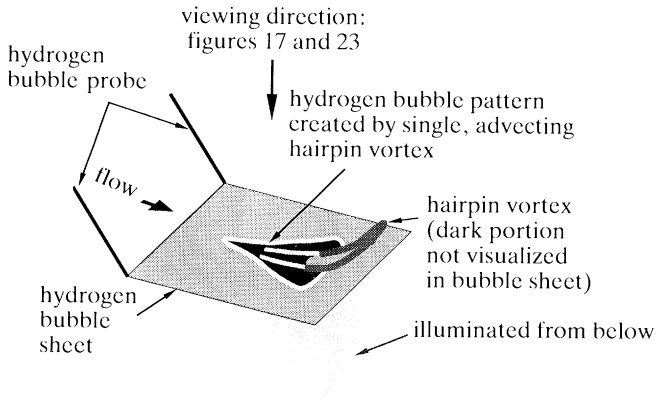

Figure 16. Schematic diagram of technique employed to visualize flow development associated with a single hairpin vortex.

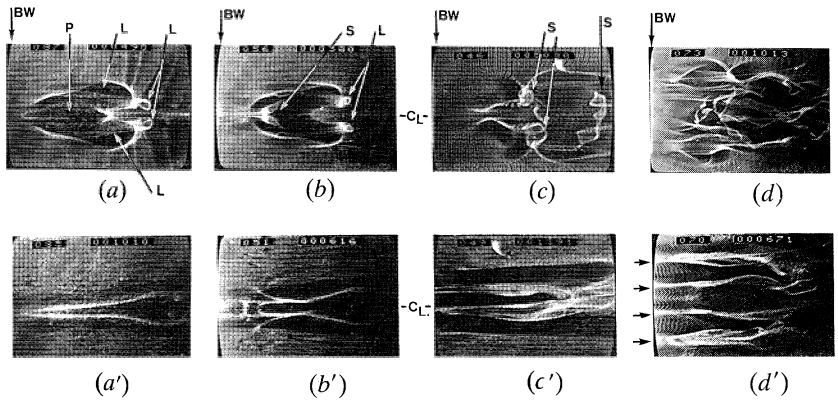

Figure 17. Dual-level, plan view visualization of hydrogen bubble patterns generated by left-to-right passage of developing hairpin vortex (cf. figure 16). BW denotes the position of the bubble wire, P the location of an initial 'pocket' formation (Falco 1991), L the location of the vortex legs, S the evolution of secondary hairpin vortices (see §5), and C_L the plane of symmetry. Bubbles are generated at $y/\delta = 0.4$ for upper row visualizations and $y/\delta = 0.1$ for lower row visualizations.

as the vortex passes by, the hairpin vortex legs (denoted by regions L in figure 17a, b) sweep the bubbles to the sides producing the clear areas in the bubble sheet. Note that these clear areas, which appear as dark regions in figure 17, are consistent with the observed 'pockets' described by Falco (1981, 1991); a typical pocket pattern is labelled P in figure 17a. Figure 17a'–d' illustrate the corresponding behaviour with the bubble wire located very near the surface, where streaks of low-speed fluid (the bright, concentrated regions in the pictures) develop beneath the passing hairpin. Note how the number of streaks present increases from one in figure 17a', when only a single hairpin is present, to four in figure 17d' (indicated by the arrow heads). By the stage shown in figure 17d (well downstream), the original hairpin has expanded laterally by both the process described in §3 and the induction of additional (secondary) hairpin vortices (labelled S in figure 17) through interactions with the surface flow (see §5).

This process of streak creation is also supported by numerical simulations of a

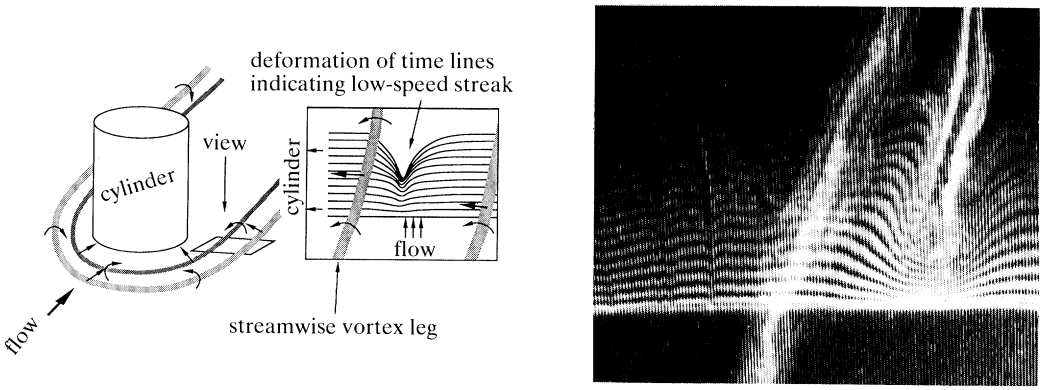

Figure 18. Plan-view of necklace vortex leg interaction to create low-speed streak. Plan-view photograph shows a streamwise necklace vortex leg (visualized by upstream hydrogen bubble wire) interacting with surface fluid (visualized by bubble wire near surface) to create low-speed streak at surface.

hairpin vortex convected in a shear flow (Hon & Walker 1987); computed trajectories of markers introduced near the surface show that they collect into long streaks with the passage of the vortex. Similar conclusions have also been reached by Robinson (1990) in his interpretation of the direct numerical simulations. Consequently, it is reasonable to conclude that the low-speed streaks represent the signature of convected outer-region vortices. This effect can be easily understood with reference to figure 2. Consider a vortex which has significant streamwise orientation, but whose axis may be skewed relative to the mean flow direction. Viewed in a frame of reference moving with the vortex core, the instantaneous induced flow pattern in the cross-vortex plane will be of the general type indicated in figure 2. Consider the nature of the flow produced in the region of outflow near B, and let B be the origin for z, measuring spanwise distance from left to right in figure 2*a*. Then for small positive z, we have $v > 0$ and $w < 0$. In the upper portion of the surface layer under B, the motion is principally inviscid. Neglecting unsteady effects, as well as streamwise variations (in x), it follows from the streamwise momentum equation that $\partial u/\partial z > 0$ when $\partial u/\partial y > 0$. Thus, a minimum in u must occur near $z = 0$ and the flow near B will be both away from the wall and retarded in the streamwise direction.

This process of low-speed streak generation is further illustrated and substantiated in figure 18 (from Greco & Smith 1991), which is a plan-view of the vortex-induced eruptive behaviour at the same streamwise location as shown in figure 5. Here the streamwise extension of a necklace vortex is visualized by bubbles from an elevated, upstream hydrogen bubble wire, and appears as a bright, concentrated region passing vertically across the centre of figure 18; the eruptive regions shown in figure 5 appear in figure 18 as a low-speed streak pattern, which is visualized with a hydrogen bubble wire located adjacent to the surface. The streak shown in figure 18 is at a stage approximately mid-way between the gently upwelling agglomeration to the left in figure 5 and the sharply eruptive spire to the right. Note that the streak region moves laterally in phase with the movement of the vortex as the theory described in §2 suggests (Walker 1978; Doligalski & Walker 1984). In addition, the streak is observed to form at a lateral location equivalent to approximately 1.5 vortex heights (from the wall) outboard of the centre of the vortex core (depending on the vortex strength). This location is consistent with the theory discussed in §2;

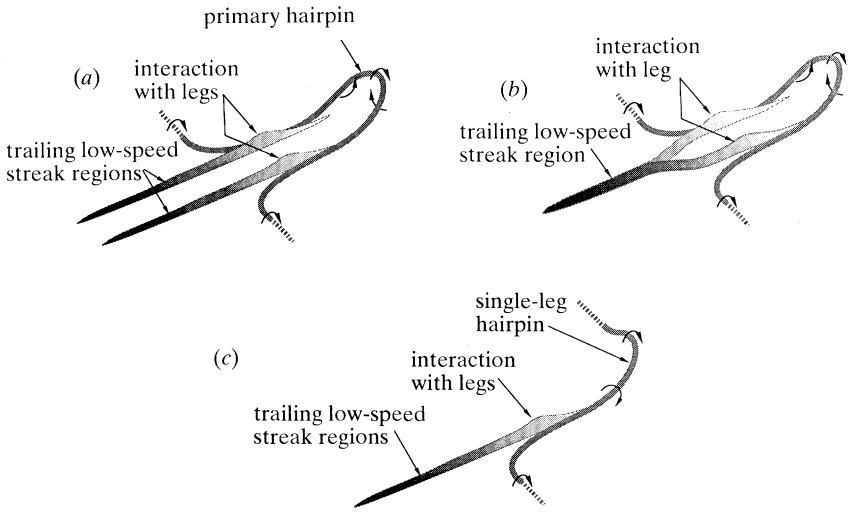

Figure 19. Schematic diagram of the processes whereby moving hairpin vortices induce low-speed streaks. (*a*) Symmetric case with wide separation of legs. (*b*) Symmetric case with legs closer together; the two streaks merge. (*c*) Asymmetric case.

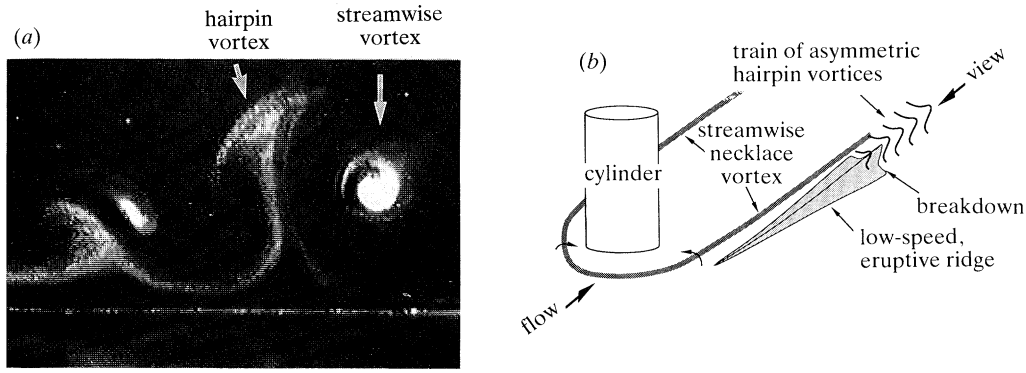

Figure 20. Characteristics of the breakdown of the eruptive spires induced by streamwise necklace vortex legs. (*a*) End-view, light-sheet photograph showing the breakdown of an eruptive spire (low-speed ridge) induced by a streamwise necklace vortex leg. (*b*) Schematic illustrating the general breakdown process for the low-speed, eruptive ridge.

the outflow stagnation point associated with the rectilinear vortex (shown at B in figure 2*a*) is $\sqrt{3}$ vortex heights, measured laterally from the vortex core (Walker 1978; Doligalski & Walker 1984). Further comparisons with low-speed streak patterns from a fully turbulent boundary layer (Greco & Smith 1991) suggest that the types of deficit pattern obtained during this interaction are indistinguishable from naturally occurring streaks, as well as displaying all of the observed streak dynamics such as streak oscillation and eventual breakdown. This breakdown process is discussed in detail in §5, where it is illustrated that the breakdown of the streak pattern results in the formation of hairpin vortices (see figure 20).

The net effect of the motion induced by both a symmetric and an asymmetric hairpin vortex is shown schematically in figure 19, where the upward motion induced by the leg of a vortex produces a trail of upwelling flow as the vortex is convected

downstream. For a symmetric hairpin vortex (Haidari & Smith 1991), where the legs are separated by a sufficient distance, two streaks are generally produced, one associated with each leg as indicated in figure 19*a* (cf. figure 17*b*′). On the other hand, when the vortex legs are sufficiently close, the two streaks are observed to merge and give the appearance of a single streak as indicated in figure 19*b* (cf. figure 17*a*′). Note that streak patterns similar to those depicted in figure 17*a*′ and *b*′ are commonly observed in turbulent wall layers. Of course, the effect is not dependent on the symmetry of the vortex, and the development for the asymmetric hairpin is shown schematically in figure 19*c*. The vortices which create the streaks are plentiful near the surface, where the streamwise velocity is high relative to typical spanwise speeds (Walker 1990*a*). Hence the streaks (or vortex trails) can be expected to be long with respect to their spanwise spacing.

Note that not every hairpin vortex in the boundary layer will produce a streak. The streaks only indicate the presence of those vortices closest to the wall; such vortices exert the dominant effect on the near-wall flow and, in effect, act to shield the wall from all other vortices above. A streak will only initiate when a vortex is brought into close proximity to the surface, normally when either a leg penetrates through the agglomeration of vortices above, or an entire vortex is recirculated down toward the surface. In contrast, a streak may terminate due to the departure of the causative vortex from the surface region. Finally, a process for regeneration of a streak has been observed (Smith 1984) wherein a new vortex from upstream can overrun an old streak (that was created by a previous vortex), causing either a refocusing or lateral movement of the streak. It is believed that the lateral oscillation and side-to-side meandering of streaks are manifestations of this interaction and refocusing of streaks, when vortices from upstream advect over existing streaks.

In general, it may be concluded that the majority of a wall-layer streak is not dynamically significant and represents essentially the passive trail of a hairpin vortex. As the streak is traced out in the wall-layer flow by a passing hairpin vortex, the leading-edge of the streak will propagate downstream in phase with the vortex at a location below the leg and to the side where the vortex-induced flow is away from the wall. When the viscous flow in the vicinity of the leading-edge region of a streak has been exposed to an adverse pressure gradient due to the vortex above for a significant period of time, it will undergo a strong viscous–inviscid interaction, and an eruptive event occurs. Note that the phenomenon develops in a frame of reference moving locally with the hairpin leg. It is this mechanism of eruption and turbulence production/regeneration which is addressed in the following section.

5. The production mechanism

Here attention is focused on the physical mechanism for regeneration of new vortices near the surface and the means by which new vorticity is introduced into the outer portion of the turbulent boundary layer. In §3 and §4, a structural model of the outer region of the turbulent boundary layer has been described wherein large numbers of hairpin vortices, of relatively small lateral extent, are convected above the viscous inner region near the wall. As discussed in §3, each hairpin vortex sends out trailing legs which evolve in the background shear flow and propagate down toward the wall. It is evident that the movement of the legs toward the surface cannot continue indefinitely. At any instant, the zone between the vortex legs and the wall is a region of thickness $O(\nu/u_\tau)$, where viscous and unsteady effects are

PHILOSOPHICAL TRANSACTIONS OF THE ROYAL SOCIETY A MATHEMATICAL, PHYSICAL & ENGINEERING SCIENCES

significant to leading order, and where the instantaneous velocity is reduced to relative rest on the wall. Thus, for any vortex in proximity to the surface, a double structure exists in the local flow field. Recall that a viscous–inviscid interaction is any event which leads to a localized breakdown of the near-wall viscous flow (or in other words, a local separation of the surface layer) and a consequent mixing or interaction between the inner and outer regions of the boundary layer. In §2, it was argued that such interactions are provoked by vortex motion above the surface. For two-dimensional flows, the interaction takes the form of a sharp spike-like eruption (Elliott *et al.* 1983) that has also been observed experimentally in a variety of situations. However, since the instantaneous flow in a turbulent boundary layer is highly three dimensional, care must be exercised in applying two-dimensional results in such situations.

Recently, Van Dommelen & Cowley (1990) have extended the theory of unsteady separation to a fully three-dimensional flow (see also Cowley *et al.* 1990) and have obtained the remarkable result that a generic structure can develop in an erupting three-dimensional shear layer as it leaves the surface. The generalization of the MRS condition is that the eruption will originate within a region of external adverse pressure gradient somewhere along a zero vorticity surface (as opposed to the zero vorticity line in two-dimensional flows). The zero vorticity surface is the locus of points within the boundary layer where both the instantaneous streamwise and spanwise vorticity vanish. Again note that viscosity is critical in triggering the entire separation process, in that a viscous layer exposed to an adverse pressure gradient will invariably develop regions of recirculating flow (and hence a surface of zero vorticity). In unsteady three-dimensional boundary layers, a wide variety of complex recirculating topologies can develop which give rise to a zero vorticity surface. Once such a surface develops, the study by Van Dommelen & Cowley (1990) suggests that an eruptive response will occur, provided the adverse pressure gradient is maintained. Viewed from above, a surface-layer eruption generally initiates along a U-shaped or crescent-shaped ridge, instead of along a knife-edge (as in two dimensions). The outward motion takes the form of an erupting tongue of fluid warped in the shape of a U, with the region of highest penetration near the bottom of the U. This three-dimensional eruption does resemble the two-dimensional case, if viewed in any plane which is both normal to the wall and to the crescent-shaped ridge; narrow 'spikes' will be observed in such a plane. At the onset of the event, the flow focusses sharply into a narrow erupting tongue. Physically what transpires is that a small region of fluid particles within the surface boundary layer becomes strongly compressed in a direction tangential to the surface. This forces the oncoming flow from upstream to be deflected around the compressed zone and, more importantly, upward toward the outer region in a sharply focused narrow-band eruption (Cowley *et al.* 1990). Prior to the onset of the phenomenon, the external (adverse) pressure gradient will have caused vorticity to diffuse outward from the wall within the surface layer. As the surface layer begins to separate, the strong streamwise compression of local fluid particles drives the constant vorticity surfaces rapidly outward. To either side of these elongated fluid particles, the constant vorticity surfaces converge to form a double-sided erupting sheet of vorticity that appears as a 'spike' in cross section (cf. figure 3*c*). (In the formal lagrangian description of the event, a specific fluid particle is compressed to zero thickness (Cowley *et al.* 1990).) By this stage, the evolution of the eruption is principally nonlinear and inviscid (Cowley *et al.* 1990). Furthermore, it is evident by the nature

PHILOSOPHICAL TRANSACTIONS OF THE ROYAL SOCIETY A MATHEMATICAL, PHYSICAL & ENGINEERING SCIENCES

of the phenomenon that very sharp changes in velocity occur across most horizontal traverses of the erupting sheet.

At present, theoretical descriptions of such eruptive events are limited to the initiation of the phenomenon (Cowley *et al.* 1990). Unfortunately, the accurate calculation of both the sharply focused eruptive phenomena and the subsequent viscous–inviscid interaction at high Reynolds number is well outside the present scope of modern computational methods. However, once the dynamics of the separation process are appreciated, it is possible to speculate on the events that occur next, as well as to investigate the nature of the interaction through careful observation of a variety of 'kernel' experiments. One such experiment has previously been described in connecton with figures 5 and 18. To observe the nature of the interaction that develops as a consequence of the rapidly erupting spires shown in figure 5, the observation position was shifted somewhat downstream as shown schematically in figure 20. It may be inferred from the end-view photograph shown in figure 20*a* that the eruptive spire interacts with the mainstream flow and rolls over, generating a mushroom-shaped pattern reflective of hairpin vortices. As shown schematically in figure 20*b*, the roll-over process results in an observed breakdown of the eruptive ridge into a continuous sequence of discrete hairpin vortices (Greco & Smith 1991). Note that the roll overs appear to be skewed outward from the vortex axis and produce asymmetric hairpin vortices.

Recently, Haidari & Smith (1991) completed an extensive set of experiments in which single, well-defined, symmetric hairpin vortices were created in an otherwise laminar boundary layer (as described in §4); the development of these hairpin vortices was then observed as they convected downstream. Many of the features discussed in §3 and §4 relating to both the interaction of a hairpin vortex with a background shear flow and the creation of low-speed streaks were observed in these experiments as the vortex moved downstream. In addition, the simple vortex-induced downwashes at the front of the vortex and the upwelling between the vortex legs that are described by Robinson (1990, 1991) were noted. However, a central object of the experimental work was to observe the original hairpin vortex in the act of regenerating another vortex through a viscous–inviscid interaction with the surface flow. It is important to appreciate that as the original hairpin vortex is convected downstream within the existing laminar boundary layer, it induces the development of an additional unsteady surface layer between itself and the wall. A goal was to isolate and determine the nature of the breakdown and the subsequent eruption of the surface layer. To accomplish this, a hydrogen bubble-wire probe, consisting of a wire that was much longer than the lateral extent of the created vortex, was positioned downstream normal to the mean flow direction and at constant height from the surface. A continuous sheet of hydrogen bubbles is released from the wire and marks the flow as the hairpin vortex passes near the probe. Since the probe could be located at any height from the wall, as well as any streamwise location, the influence of the hairpin vortex on the surrounding flow field could be observed from a number of perspectives. The injection at the surface was computer-controlled (as shown in figure 14) and the hairpin vortices created in this manner were highly repeatable (see figure 15). A schematic illustrating the method of observation of the effect of the hairpin vortex on the hydrogen bubble sheet is shown in figure 16.

As a hairpin vortex is convected downstream, the regeneration of new hairpin vortices by the interaction of the original hairpin vortex with the surface flow is

PHILOSOPHICAL TRANSACTIONS OF THE ROYAL SOCIETY A MATHEMATICAL, PHYSICAL & ENGINEERING SCIENCES

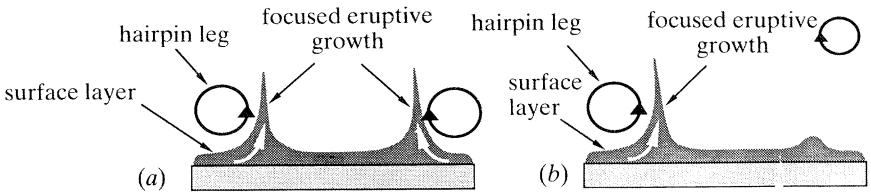

Figure 21. Schematic diagram of location of vortex-induced separation of the surface layer for symmetric and asymmetric hairpin vortex legs.

clearly observed (Haidari & Smith 1991). The onset of the process is entirely consistent with the theoretical description of unsteady three-dimensional separation of the surface layer beneath the vortex (Van Dommelen & Cowley 1990). However, the dynamics of the event are complicated and take place abruptly. Thus careful positioning of the hydrogen bubble probe at several streamwise locations is required to observe the discrete eruption that leads to the evolution of new hairpin vortices. To facilitate the interpretation of the physics, the flow processes were observed from different perspectives by systematically varying the height of the bubble wire from the wall. In what follows, a detailed description of the regeneration process will be given using a series of schematic diagrams and accompanying photographs from the experiments (Haidari & Smith 1991). It should be noted that the details of the process are complex. From an experimental perspective, a firm appreciation of the theoretical framework recently established for unsteady separation (Cowley *et al.* 1990) is a key element in knowing where to look for the critical events in the experiments and properly interpreting the observations.

Consider first a symmetric hairpin vortex that is being convected near a wall. In the cross-vortex plane (cf. figure 2), the motion is similar to a pair of counter-rotating vortices with an adverse pressure gradient induced near the surface in the lateral direction inboard of the legs. Once the surface flow has been exposed to this local lateral pressure gradient, sharply focused eruptions are anticipated in the locations indicated in figure 21*a* (Ersoy & Walker 1985). For an asymmetric hairpin vortex (with or without a second leg), the eruptive response will be induced by the vortex closest to the wall as in figure 21*b* (Ersoy & Walker 1986). It should be emphasized that the events sketched in figure 21 are not meant to depict the simple vortex-induced upwelling described, for example, by Robinson (1990); rather the schematic implies a sharply focused, discrete eruption that occurs only after the viscous flow has been exposed to a pressure distribution associated with the vortex above for a period of time. The schematics of figure 21 are useful in delineating the general vicinity of the surface-layer eruption, but it must be remembered that the hairpin vortex is a fully three-dimensional structure, a point which is considered next.

As a symmetric hairpin vortex (shown in figure 22) moves adjacent to a wall, an unsteady viscous flow develops beneath it, which is driven by the pressure field induced by the vortex. In the region between the vortex legs and behind the vortex head, the pressure gradient is adverse (in both the streamwise and lateral directions), and the persistent action of this pressure gradient can be expected to give rise to regions of three-dimensional recirculation that develop in a frame of reference moving with the vortex (Walker 1978; Doligalski & Walker 1984). Note that a wide variety of complex topologies may be anticipated in the surface flow. Falco (1991) indicates that he has observed so-called 'pocket vortices' near the surface, which appear to be associated with a primary vortex farther from the surface. At present,

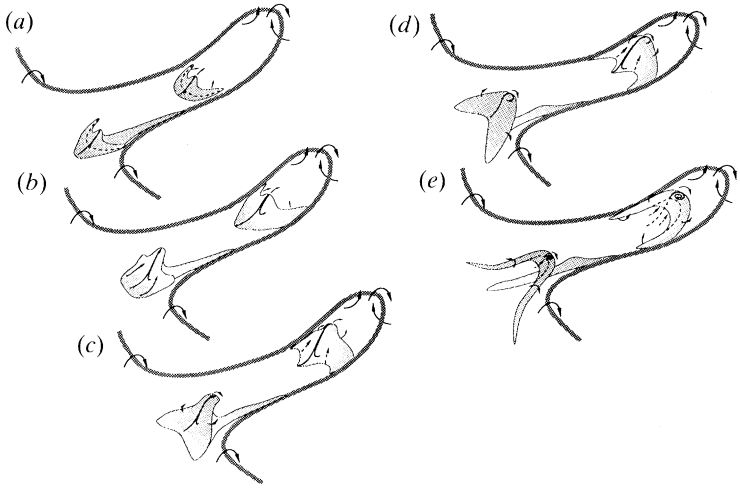

Figure 22. The generation of secondary vortices via surface interaction for a symmetric hairpin vortex. (*a*) The onset of interaction; sharp, crescent-shaped ridge develops in the surface flow where the induced pressure gradient near the surface is adverse. (*b*) Rapid outward movement of the erupting ridge which contains concentrated vorticity. (*c*) The erupting sheet starts to roll over. (*d*) Partial roll-over reached. (*e*) Complete generation of secondary hairpin vortices.

details of the various surface-response topologies that can occur in general three-dimensional flows are not well documented (see, for example, the review by Cowley *et al.* (1990)), but the evolution of a surface of zero vorticity is anticipated in a region of adverse pressure gradient. Consider first the region near the vortex head in figure 22. In any plane normal to the wall and parallel to the streamwise direction, the hairpin vortex will appear as a convected transverse vortex that induces a translating local adverse pressure gradient near the surface behind the vortex head (cf. figure 2 and Doligalski & Walker 1984). Although the vortex head is usually farther from the wall than the rest of the vortex, the level of adverse pressure gradient is strengthened in the region behind the vortex head by the spanwise flow induced by the vortex legs. It is within this region that an eruptive surface response is anticipated. On the other hand, separation of the surface layer is also expected in two other locations for the symmetric vortex configuration shown in figure 22. Recall that the closer a vortex is to the wall, the more rapid the eruptive boundary-layer response (Doligalski & Walker 1984); generally, the trailing vortex legs make the closest approach to the wall. Indeed, as discussed in §3, the trailing legs will continue to move closer to the wall in a shear flow until their progress is arrested either by dissipation, or if a surface eruption is induced. Again, the lateral pressure gradient induced by a trailing leg is adverse inboard of the leg (cf. figure 2). Consequently, for the symmetric hairpin vortex configuration shown in figure 22, an eruption of the surface layer is expected in three locations, namely behind the vortex head and near each trailing leg. For simplicity the sequence of events near only one trailing leg is shown in figure 22; however, the following description of the surface behaviour applies to all three locations (albeit at different times).

In a frame of reference moving with a section of the vortex, separation of the surface layer below the vortex initiates along what appears as a U-shaped ridge (looking down from above) with the top of the U facing downstream. The orientation

of the eruptive ridges relative to the hairpin vortex is shown in figure 22*a*. Each ridge is narrow, contains elevated levels of vorticity, and is farthest from the wall near the bottom of the U (Van Dommelen & Cowley 1990). The broken lines in figure 22*a* denote the downstream base of the crescent (hidden by the erupting ridge), while the small solid lines represent the shape of the erupting surface in a cross section through the ridge (see also figure 22*b*). Note that the stage shown in figure 22*a* is a relatively mature phase of the separation process described by Van Dommelen & Cowley (1990); the schematic diagram is also not to scale. As the erupting sheet of surface layer fluid rises, it rapidly penetrates regions of ever increasing streamwise velocity, as suggested in figure 22*b*. The expected behaviour is that a rollover of the sheet will occur, starting from the tip of the tongue and spreading outboard along the rest of the ridge. The initiation of this phase is shown schematically in figure 22*c*, where the erupting surface layer appears as a thin cowl in the shape of a cobra head poised to strike. The next stage of the process is depicted in figure 22*d* where a majority of the sheet has rolled up. The final stage of regeneration is shown in figure 22*e* where ejection from the surface layer is complete, along with the formation of new secondary hairpin vortices containing the concentrated vorticity that originated in the surface layer. Note that as the erupting ridge rolls up and detaches from the surface layer, a sweep event will occur, approximately between the stages indicated in figure 22*d* and *e*. The sequence of events illustrated in figure 22 constitutes a strong unsteady viscous–inviscid interaction. Once the generation of the secondary hairpin vortices is complete, as indicated in figure 22*e*, an inner and outer structure to the flow is quickly re-established. The newly formed hairpin vortices may intertwine with the parent vortex, as discussed in §3, or alternatively can act to induce further breakdowns of the wall-layer flow downstream, thereby producing further hairpin vortices. It should be noted that the process described here is consistent with (and provides a dynamical explanation of) the evolution of 'new vortical arches' near 'quasi-streamwise vortices', as described by Robinson (1990).

The process depicted schematically in figure 22 may be seen in the sequence of plan-view photographs in figure 23 (from Haidari & Smith 1991), which shows the influence of an initial single hairpin vortex created by the injection process described in §4, and shown in figures 15 and 17. In this sequence, the hydrogen bubble probe depicted in figure 16 has been placed close to the surface at a downstream location appropriate for viewing the development of the regeneration process; the view in figure 23 is from above. In figure 23*a*, the parent hairpin vortex has arrived in the vicinity of the field of view, with the hairpin head well above the bubble sheet at approximately the streamwise position indicated by HPH. The clear regions to the left, labelled A, are where the legs of the hairpin pass through the plane of the bubble sheet. The vortex-induced flow sweeps the bubbles away, and the clear zones effectively mark the local outline of the cores of the vortex legs. At the next instant, shown in figure 23*b*, the parent hairpin vortex has moved farther to the right, and the outline of a small eruptive tongue is just visible at the location marked B; this erupting ridge corresponds to that shown schematically behind the vortex head in figure 22. Because of the repeatability of the experiment, as well as the placement of the hydrogen bubble wire, it can be categorically stated that the erupting ridge originates from the surface flow. With the passage of time, the eruptive ridge moves rapidly outward and, as may be inferred from figure 23*c–g*, the phenomenon takes place in a frame of reference moving with the parent hairpin vortex. A process of rollup from the tip of the erupting tongue is clearly underway by the stage shown in

PHILOSOPHICAL TRANSACTIONS OF THE ROYAL SOCIETY A MATHEMATICAL, PHYSICAL & ENGINEERING SCIENCES

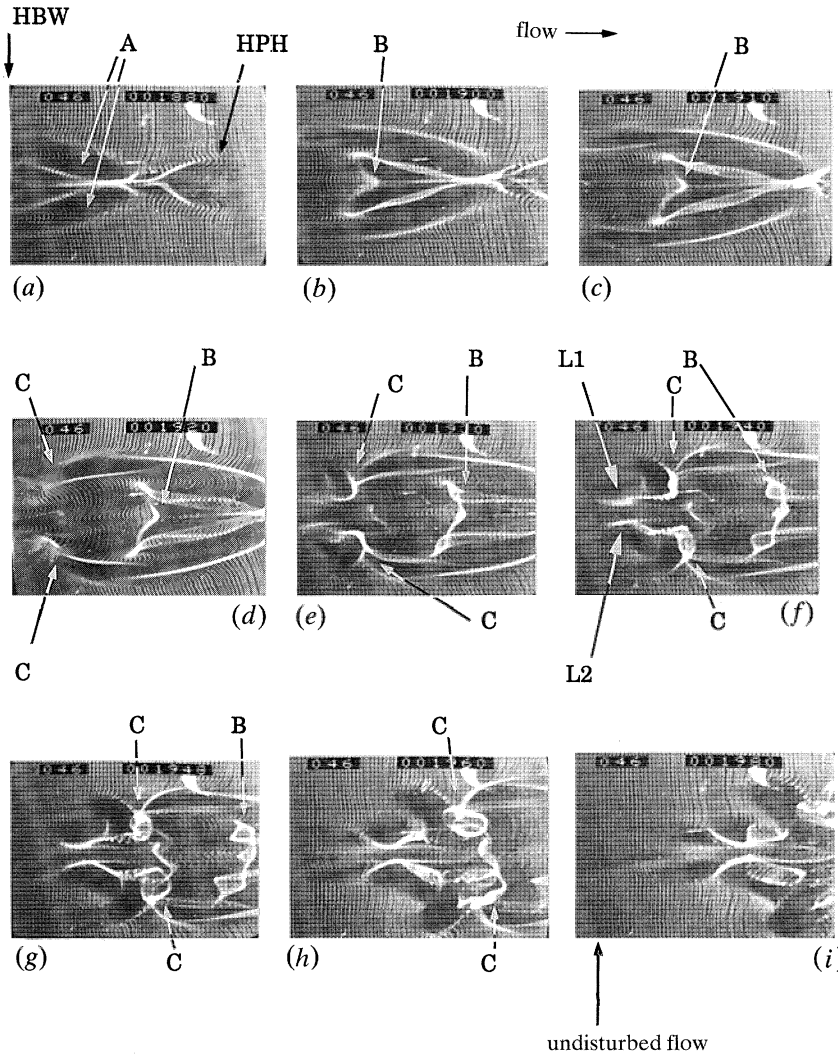

Figure 23. Plan-view hydrogen bubble wire visualization sequence illustrating the development of secondary vortices near the surface as a primary hairpin vortex passes a fixed streamwise location. HBW denotes the position of the hydrogen bubble wire, HPH is the location of head of primary vortex, A the location of the trailing legs of primary vortex, B the development of a secondary vortex behind head of primary, C the development of secondary vortices adjacent to the legs of the primary vortex, and L1, L2 the legs nearest the symmetry plane for the secondary vortices indicated by C. (*a*) $t = 0$ s; (*b*) $t = 0.166$ s; (*c*) $t = 0.25$ s; (*d*) $t = 0.33$ s; (*e*) $t = 0.146$ s; (*f*) $t = 0.5$ s; (*g*) $t = 0.58$ s; (*h*) $t = 0.666$ s; (*i*) $t = 0.833$ s.

figure 23*e*. However, by this stage the beginning of a similar process of surface eruption and roll-up near the trailing vortex legs may now be seen at the locations labelled 'C' in figure 23*d*. As may be observed in figure 23*f–h*, three new hairpin vortices have been induced through an interaction with the surface flow (in the manner depicted in figure 22) and continue to grow and move farther from the wall.

The hairpin vortices labelled 'C' in figure 23 were originally interpreted to be subsidiary vortices by Smith *et al.* (1990) (i.e. distortions in the parent vortex produced through interaction with the background shear flow, as described in §3).

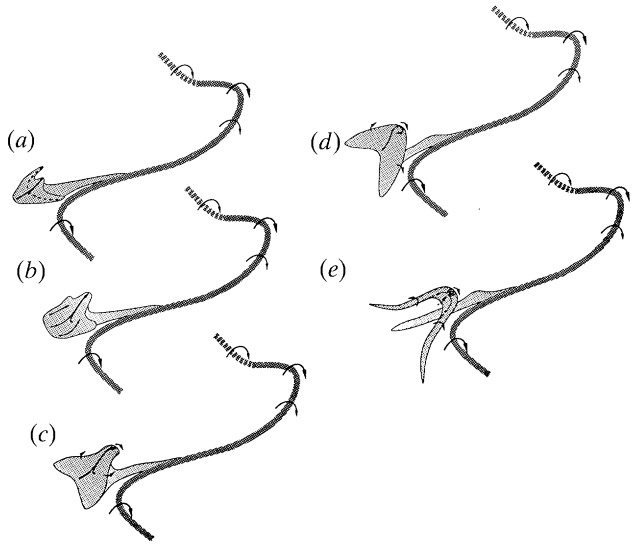

Figure 24. The generation of secondary vortex via surface interaction for an asymmetric hairpin vortex. (*a*) The onset of interaction; sharp, crescent-shaped ridge develops in the surface flow where the induced pressure gradient near the surface is adverse. (*b*) Rapid outward movement of the erupting ridge which contains concentrated vorticity. (*c*) The erupting sheet starts to roll over. (*d*) Partial roll-over reached. (*e*) Complete generation of secondary hairpin vortex.

However, closer examination of the detailed visualization results (Haidari & Smith 1991) suggests that both of the new hairpin vortices are produced through an eruption of the surface flow near the trailing legs, as indicated in figure 22, and are therefore secondary hairpin vortices. A closer examination of figure 23 reveals an interesting difference between the process that occurs behind the parent vortex head and the process adjacent to the trailing legs. The rollup 'B' that occurs behind the vortex head occurs principally in the streamwise direction and yields a new secondary hairpin with the same orientation as that of the parent hairpin vortex. On the other hand, the eruptive process that gives rise to the formation of the secondary hairpins 'C' near the trailing legs occurs along a ridge that is skewed inward toward the plane of symmetry of the parent hairpin vortex. Thus, as the new hairpin vortices 'C' form, they are skewed relative to the streamwise direction.

A further feature of the process shown in figure 23 is that the surface interaction leading to the generation of new secondary vortices produces hairpins which are initially almost symmetric (and of the type discussed by Theodorsen (1952)). The nature of the process involved in the evolution of such vortices (see also Cowley *et al.* 1990) would indicate that these vortices should be almost symmetric at birth. However, the skewed orientation of the vortices labelled 'C' in figure 23, as well as the processes described in §3, which favour the development of asymmetric vortex configurations in a highly sheared environment, suggest that most hairpin vortices in the turbulent boundary layer will soon develop the asymmetric shape depicted in figure 24. However, with regard to the regeneration process, the question of symmetry or asymmetry in the parent hairpin vortex is not important, since either configuration results in strong surface-layer eruptions; for completeness the regeneration process for an asymmetric hairpin vortex is shown schematically in figure 24.

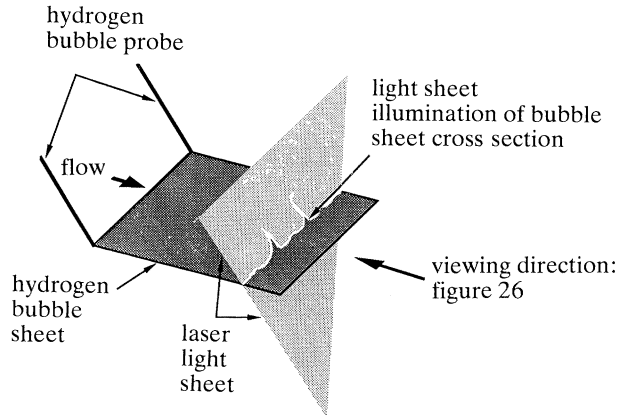

Figure 25. Schematic diagram of laser sheet visualization technique used to visualize eruptive events in a turbulent boundary layer.

The vortex structures shown in figure 23 are induced by a single hairpin vortex. As these cumulative flow structures move downstream, further induced eruptions and new secondary hairpin generation are observed (Haidari & Smith 1991). Consequently, through both a series of viscous–inviscid interactions with the surface flow and the process of lateral growth described in §3, the original hairpin is observed to spread and grow into a turbulent spot. Beneath the growing patch of turbulence, low-speed streaks are observed (Haidari & Smith 1991), as well as continual processes of discrete eruptive activity (e.g. figure 17*d*) that appear to be generated by agglomerations of hairpin vortices which comprise the internal structure of the turbulent spot.

6. Discussion

In this paper, several fundamental physical mechanisms related to the dynamics of turbulence near a wall have been described, generally based on the hypothesis of the hairpin vortex as a key structure of the turbulent boundary layer. It is argued here that an appreciation of the basic dynamics of hairpin vortices now allows a reasoned interpretation of the observed behaviour for both transitional and fully turbulent shear flows. For example, in transitional flow it is evident that once hairpin vortices are in proximity to a surface, originating either from a process of Tollmein–Schlichting wave amplification or from vorticity contamination of the mainstream flow (i.e. bypass transition (Morkovin 1969)), such vortices will generate new vortices at the surface via the process described in §5 (provided the external velocity is sufficiently large). The entire process grows and feeds on itself in the manner illustrated by Haidari & Smith (1991), spreading in the spanwise direction until a fully turbulent state is achieved at some downstream location. By this stage, the number of eruptions of the surface flow must reach some self-sustaining asymptotic value per unit time and per unit area of the wall.

The sharp narrow band eruptions can also be observed in a fully turbulent flow, but only through innovative flow visualization techniques. One approach is shown schematically in figure 25, which uses a sheet of hydrogen bubbles generated very close to the wall in a fully turbulent boundary layer and illuminated by a cross-stream laser sheet located a short distance downstream. The resultant pictures are

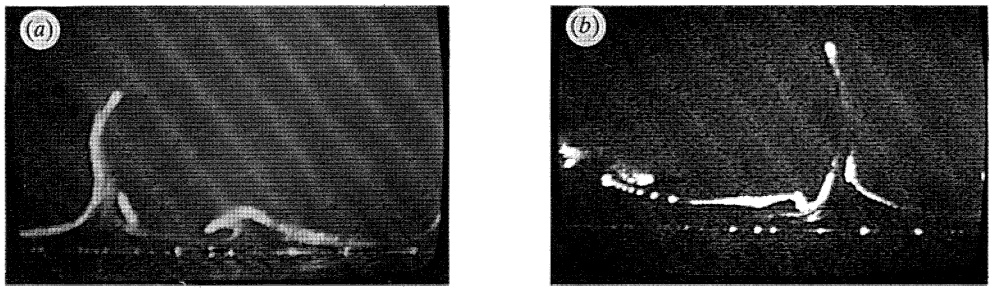

Figure 26. End-view visualization, using a horizontal hydrogen bubble wire and laser light-sheet illumination (see figure 25), showing eruptive spires emanating from near-wall region of a turbulent boundary layer ($Re_\theta \approx 1150$). Lateral yield of view *ca.* 250 wall units, wire located $y^+ = 7$ from surface, and $x^+ \approx 150$ upstream of light sheet. Compare with eruptions induced by streamwise vortex as shown in figure 5. Tip penetration: (*a*) $y^+ = 92$; (*b*) $y^+ = 105$.

cross-stream 'slices' of the deformed bubble sheet. Typical visualizations are shown in figure 26 for a turbulent boundary layer developing on a flat plate in a water channel at a Reynolds number based on momentum thickness of $Re_\theta \approx 1150$. The boundary layer was tripped near the leading edge to achieve a fully turbulent flow.

In figure 26, the hydrogen bubble wire was located at a distance of $y^+ = 7$ from the wall. The laser sheet was positioned approximately 150 wall layer units downstream of the bubble wire. Note the thin eruptive spires that are visible in the laser sheet. The tips of these spires were observed to penetrate to heights above the surface ranging typically from $y^+ = 60$ to $y^+ = 150$. In figure 26*a* and *b* the tips of the spires are at $y^+ \approx 92$ and $y^+ \approx 105$, respectively. Note that similar eruptive events have also been observed for a turbulent boundary layer in air using smoke injection and laser sheet illumination (Wallace & Balint 1990). Three points should be emphasized. First, there is no doubt that the eruptive spires shown in figure 26 originate near the surface, since the hydrogen bubbles are introduced very close to the wall and a short distance from the laser sheet; consequently, a strong, focused upward motion is necessarily implied. Secondly, the events captured in figure 26 are the result of localized breakdowns of the wall-layer flow and subsequent strong interaction with the outer flow. Such events are not infrequent; detailed review of video recordings of these views reveals that this type of eruptive event occurs repeatedly, with the spires appearing intermittently at random spanwise locations (also confirmed by Wallace & Balint (1990)). Lastly, the breakdowns depicted in figure 26 are the only type of eruptive event observed in the laser sheet. Note the lateral thinness of the spires; the lateral field of view in figure 26 is about 250 wall units and the spires typically have a width of about 5 or less wall units. Theory suggests that these eruptive spires contain high levels of vorticity (Van Dommelen & Cowley 1990) and involve sharp changes in vorticity along any horizontal traverse. It therefore seems unlikely that such phenomena can be adequately resolved using current direct numerical simulation methods.

The physical origin of these eruptive spires is hypothesized to be consistent with the process described in §5. During the evolution of secondary hairpins near the legs of the parent hairpin vortex (cf. figures 22 and 24), it was noted that the process initiates from a rapidly rising, thin eruptive cowl, which eventually appears to roll inward and away from the leg to form a secondary hairpin. The end result of this process may be seen in figure 23 where the secondary hairpins that evolve near the

PHILOSOPHICAL TRANSACTIONS OF THE ROYAL SOCIETY A MATHEMATICAL, PHYSICAL & ENGINEERING SCIENCES

legs are slanted inward toward the symmetry axis of the parent hairpin vortex. Most new hairpin vortices are anticipated to develop in this manner (provoked by asymmetric vortices). The most plausible explanation for the thin spires is that they represent a slice through the eruptive cowl which is caught at that instant in the laser sheet. The nature of the event depicted in figures 22 and 24 is such that, when viewed in most planes which are normal to the wall, a thin spire will be seen; the eruptive zone will only appear to have appreciable thickness when viewed from the side of the cowl.

In this paper we have presented an overall model of the detailed processes that occur near the surface in a turbulent boundary layer. An appreciation of the basic dynamics near the surface suggests new modelling approaches for the prediction of mean-flow quantities (see, for example, Walker *et al.* 1989; Walker 1990*b*; He *et al.* 1990; Degani *et al.* 1991), particularly for the wall-layer flow. As described in this paper, lasting contributions to the mean Reynolds stress near the wall are made during intermittent, relatively short-duration breakdowns of the wall-layer flow. These events involve sharply focused surface-layer eruptions and the subsequent roll-up of sheets of vorticity; at present, the evolution of such phenomena cannot be reliably computed for high Reynolds number. Consequently, direct modelling of the mean Reynolds stress, in which the dynamics of the wall layer are tied directly to mean quantities, appears to be a formidable task. Walker *et al.* (1989) discuss an alternative approach for modelling the near-wall flow, in which representative motions are considered during the relatively long intervals of time when the near-wall flow is quiescent, since the majority of contributions to the mean velocity profile occur during such quiescent periods. A time average over a typical cycle then produces a model for the mean velocity profile within the wall layer. Asymptotic theory shows that a mean profile model is all that is required to define a predictive approach for the wall layer for attached turbulent flows (Walker *et al.* 1989, 1991). Note, however, that direct modelling of the Reynolds stress appears to be necessary for the outer region and this is a far more complex issue. In the dynamical picture described here, the outer region is fed by intermittent sharp injections of concentrated vorticity from the near-wall zone; the challenge is to represent this dynamical behaviour by a mean Reynolds stress model.

We now consider the issues of why the mean velocity profile is observed to contain an apparently universal logarithmic behaviour near the surface and how this behaviour is associated with the present model of the dynamics. Consider a particular streamwise location and assume that the instantaneous streamwise velocity for large values of y^+ can be represented during a large majority of the time (the quiescent period) by a general expression of the form

$$u/u_\tau = u^+(x^+, y^+, z^+, t^+) \sim m(x^+, z^+, t^+) \ln y^+ + C(x^+, z^+, t^+) \ldots, \tag{9}$$

where (x^+, z^+) are streamwise and lateral coordinates, and t^+ is time scaled in wall-layer variables; m and C may be viewed as arbitrary functions of the indicated variables whose average values are κ^{-1} and C_i (cf. equation (5)). For large y^+, the fluctuating velocity u' is given by

$$u'/u_\tau \sim \{m(x^+, y^+, t^+) - 1/\kappa\} \ln y^+ + C(x^+, z^+, t^+) - C_\mathrm{i} + \ldots. \tag{10}$$

Recently, Lu & Smith (1988, 1991) obtained an extended sequence of quasi-instantaneous quantitative velocity profile measurements along a line normal to the

wall within a turbulent boundary layer by the use of image-processing of hydrogen bubble visualization. By deleting the mean component from the instantaneous velocity, profiles of the fluctuating velocity u' were established. These profiles of u' show no evidence of logarithmic behaviour for large y^+. The important implication of these results is that the instantaneous streamwise velocity field near the surface must contain a persistent logarithmic component of essentially constant slope (i.e. $m \approx 1/\kappa$). This feature of the time-dependent flow behaviour is also confirmed indirectly by well-accepted measurements of $\overline{u'^2}$; it follows that if m is significantly different from κ^{-1} over time, $\overline{u'^2}$ would have to increase proportionally to $\ln^2 y^+$ for large y^+, instead of the flat to gradually decaying behaviour observed. This behaviour is inherent in the simplified model of the wall layer described by Walker *et al.* (1989), where a logarithmic instantaneous streamwise profile is implicitly assumed for large y^+ during the relatively long quiescent state preceding breakdown of the wall-layer flow.

Over the years many arguments have been advanced to explain the observed logarithmic behaviour of the streamwise profile near a wall. Most of these arguments are not entirely satisfactory, and none reflect the nature of the near-wall dynamics. We are unable to explain why the form of the profile is precisely logarithmic in y, but we suggest that the logarithmic shape is consistent with the dynamics discussed in this paper. Near-wall turbulent flows experience cyclical local breakdowns which we have argued are the result of discrete, vortex-induced eruptions of low-speed fluid from the surface. It is evident that these eruptions must be balanced by a subsequent penetration or sweep of relatively high-speed fluid toward the surface. When this sweeping action occurs, the local instantaneous streamwise profile near the surface becomes very full, and approaches a shape closely approximated by logarithmic behaviour very near the surface (see the instantaneous profiles shown in Walker *et al.* (1989)). Initially, the high-speed sweep dominates the near-wall motion, but with increasing time the inner region thickens due to viscous diffusion, and the logarithmic behaviour is continually displaced farther from the surface. This cycle, consisting of a highly accelerated flow that subsequently relaxes away from the surface, may clearly be seen in the ensemble-averaged profiles of Blackwelder & Kaplan (1976), as well as the instantaneous measurements of Lu & Smith (1985, 1988). This behaviour is also captured in the simplified model of the wall layer described by Walker *et al.* (1989).

The logarithmic profile shape appears to be characteristic of most situations where unsteady surface-layer eruptions occur. Blair (1991) reports that immediately after an eruption in a transitioning boundary layer, the local streamwise profile shape rapidly becomes logarithmic near the surface; there then ensues a relatively long period of time where the profile relaxes back to the ambient laminar shape. Similar behaviour was reported by Greco & Smith (1991) within the end-wall boundary layer for the region shown in figures 5 and 20; their measurements show that in the lateral regions of the end wall, where periodic surface eruptions induced by the streamwise portions of the necklace vortices occur, the time-mean streamwise velocity profiles become markedly logarithmic.

We conclude by brief consideration of two passive influences on turbulent boundary layers, namely streamwise grooves and pressure gradients, which are known to have significant effects on the near-wall turbulence dynamics. First, riblets (or long streamwise surface grooves) are known to decrease the bursting rate near the surface (Wallace & Balint 1987), by inhibiting momentum exchange normal to the

PHILOSOPHICAL TRANSACTIONS OF THE ROYAL SOCIETY A MATHEMATICAL, PHYSICAL & ENGINEERING SCIENCES

wall, resulting in reduced surface shear and consequently net surface drag reduction. A grooved surface behaves, in a sense, like a cross-stream fence which significantly inhibits lateral movement of near-wall fluid. An expected consequence of restricted lateral movement in the surface flow is that the imposed adverse pressure gradient, due to the convecting hairpin legs, is less effective in generating local vorticity concentrations. Since such concentrations are necessary for the generation of eruptive surface activity, this process is retarded by the riblets, resulting in a reduction in the number and frequency of eruptions. This effect is reflected by a wider spacing of the low-speed streaks (Bacher & Smith 1986) and a decreased number of burst and sweep events. The cumulative effect is reduced momentum exchange adjacent to the surface, which results in the consequent reduction of surface drag.

Now consider the influence of a pressure gradient. It is well known that the bursting activity at the surface increases in an applied adverse pressure gradient and diminishes in a favourable pressure gradient (Kline *et al.* 1967). If a favourable pressure gradient is sufficiently large, bursting ceases entirely and relaminarization occurs. It can be argued that this behaviour is consistent with the present model; the reason is associated with a phenomenon described by Doligalski & Walker (1984). These authors considered a two-dimensional rectilinear vortex convected in a uniform flow speed of U_∞ near a wall. The vortex moves with speed $V_c = \alpha U_\infty$, where α is the fractional convection velocity such that $0 < \alpha < 1$; α decreases for either an increased vortex strength or increased vortex proximity to the wall. The magnitude of α was found to be critical in determining the precise nature of the surface-layer response, a point which is most easily understood in a frame of reference which convects uniformly with the vortex. In the moving reference frame, the wall appears to move to the left with speed V_c. The inviscid velocity induced near the surface by the vortex is also to the left, and reaches an absolute maximum speed directly under the vortex core, denoted here by U_v. The nature of the boundary-layer response is determined by whether V_c is greater than U_v or not; for a rectilinear vortex, the critical situation (i.e. $U_v = V_c$) occurs when $\alpha = 0.75$. For $\alpha < 0.75$, recirculating eddies will develop in the surface flow, followed by a subsequent 'spike-like' eruptive response, as described in § 2. However, as the advective speed V_c of a vortex increases, the time required to provoke an eruption increases. At $\alpha = 0.75$, a critical level is reached where the convection speed of the vortex is sufficiently high such that a zero vorticity line never develops in the boundary layer; at this stage U_v exactly balances the wall speed in the convected frame. For situations with $\alpha > 0.75$, the wall moves to the left faster than any velocity induced by the vortex; in such situations, the outflows from the boundary layer become much more gradual, losing their 'spike-like' character.

Thus it is conjectured that an adverse (favourable) external pressure gradient simply decelerates (accelerates) the advection of hairpin vortices relative to the wall. This change in advection rate may be thought of as increasing or reducing the time a section of the surface flow is exposed to a moving hairpin vortex in an adverse or favourable pressure gradient, respectively. The influence of this modification is thought to be most important for the portions of the hairpin where the vortex makes its closest approach to the surface near the ends of the trailing legs. Thus, for a favourable mainstream pressure gradient, the legs may be progressively accelerated beyond the threshold where a sharp (spike-like) surface response can be initiated; the legs are thereby rendered less effective in promoting a breakdown of the surface

PHILOSOPHICAL TRANSACTIONS OF THE ROYAL SOCIETY A MATHEMATICAL, PHYSICAL & ENGINEERING SCIENCES

layer. If the acceleration due to the favourable pressure gradient is sufficiently large, the effect may be enough to degrade the regenerative process at the surface to the point where relaminarization occurs. On the other hand, for an adverse pressure gradient, the hairpin vortex (particularly the leg) is decelerated. Thus the local time of exposure of the surface flow to the influence of the vortex legs is increased, which facilitates more rapid development of sharp eruptive activity from the surface. The overall effect is a more rapid and apparently more chaotic breakdown of the surface flow, as adverse pressure gradients are known to promote.

7. Summary and conclusions

A detailed model has been presented which describes the fluid dynamics of momentum exchange in the near-wall region of a turbulent flow. The key element in the model is the hairpin vortex, which is argued to manifest the physics necessary to explain both the regeneration of new vortices and the observed growth to larger scales farther from the wall. It has been demonstrated that hairpin vortices can form both within the vorticity field above the wall and by viscous–inviscid interactions with the surface flow. For the first process, it is shown that even small regions of local concentration and high curvature in the vorticity field above the surface will develop into hairpin vortices in the presence of a shear flow. Once a hairpin vortex forms, side-lobe subsidiary vortices can then develop, which retain the basic hairpin shape and act to promote lateral growth of the overall flow structure. The degree of vortex growth and deformation is critically dependent on the level of the local shear. The legs of a hairpin vortex will move rapidly toward the surface, with the spacing between the legs diminishing as the vortex penetrates into regions of increasing shear near the wall. On the other hand, the hairpin head will rise away from the surface into regions of markedly reduced shear, where strong lateral expansion of the head occurs, leading to a growth in scale. An additional mode of growth to larger scale appears to be due to hairpin coalescence, which the present studies suggest involve complicated processes of vortex amalgamation, as well as vortex breaking and reconnection.

The second process of hairpin evolution is also the mechanism of turbulence regeneration at the surface, which controls the manner in which new vorticity from the wall region is intermittently introduced into the outer region of the boundary layer. Behind the head and inboard of the legs of a convected hairpin vortex, the local pressure gradient induced near the surface by the moving vortex is adverse. The persistent action of this adverse pressure gradient soon leads to a focusing or concentration of vorticity near the wall, which is rapidly followed by an eruption (or separation) of the surface layer. The process is characterized by ejection of narrow, eruptive ‘spires’ of low-momentum fluid from the surface that contain strong concentrations of vorticity; it represents a local breakdown of the wall-layer flow that culminates in a strong viscous–inviscid interaction in which the eruptive ‘spires’ ultimately roll up into secondary hairpin vortices. This roll-up process constitutes the final stage in the intermittent ejection of concentrated vorticity from the near-wall region. Note that the closer the parent vortex is to the wall and/or the stronger the vortex is, the more rapidly the eruptive process occurs. Thus the eruptive process initiates most often near the trailing legs of the hairpin vortex.

During the initial generation process, the secondary hairpin vortices are almost

PHILOSOPHICAL TRANSACTIONS OF THE ROYAL SOCIETY A MATHEMATICAL, PHYSICAL & ENGINEERING SCIENCES

symmetric structures. However, it is demonstrated that in a highly sheared environment even a small degree of local asymmetry rapidly leads to much greater asymmetry for either a single vortex or an amalgamation of vortices. Thus, the majority of vortices in a turbulent boundary layer will be asymmetric or one-legged hairpins, with symmetric hairpins appearing (or surviving in that shape) relatively infrequently.

It has been shown that the characteristic low-speed streaks are the traces of a vortex interaction with the wall-layer fluid. The majority of a given streak is relatively inactive, except that portion immediately adjacent to the causative hairpin vortex; in this active region, the adverse pressure gradient associated with the hairpin vortex eventually provokes the development of a surface-layer eruption with a subsequent roll-over into a new hairpin vortex.

Collectively, the coupled mechanisms of vortex deformation and viscous–inviscid surface interaction provide the physics necessary to explain observed and measured turbulent boundary-layer behaviour in the near-wall region. While work still continues to clarify the growth processes that yield the larger, outer-region flow structures, the present model appears to be self-consistent with both theory and experiments, as well as the kinematical behaviour observed in low-Reynolds-number direct numerical simulations. The model thus appears to describe the appropriate physics upon which to formulate both future predictive techniques and more effective control approaches for turbulent boundary layers.

The authors thank J. P. Fitzgerald and J. J. Greco for their contributions to the end-wall interaction results presented in this paper and A. T. Degani for useful criticism of a draft of this paper. This work was supported by AFOSR under Grant no. 89-0065; the authors also express their appreciation to R. Smith, L. Ormand, M. Francis and J. M. McMichael for their patient support and encouragement during the long period over which this research took place.

References

Acarlar, M. S. & Smith, C. R. 1987*a* A study of hairpin vortices in a laminar boundary layer. Part 1. Hairpin vortices generated by a hemisphere protuberance. *J. Fluid Mech.* **175**, 1–41.

Acarlar, M. S. & Smith, C. R. 1987*b* A study of hairpin vortices in a laminar boundary layer. Part 2. Hairpin vortices generated by fluid injection. *J. Fluid Mech.* **175**, 43–83.

Aref, H. & Flinchem, E. P. 1984 Dynamics of a vortex filament in a shear flow. *J. Fluid Mech.* **148**, 477–497.

Aubrey, N., Holmes, P., Lumley, J. L. & Stone, E. 1988 The dynamics of coherent structures in the wall region of a turbulent boundary layer. *J. Fluid Mech.* **192**, 115–173.

Bacher, E. V. & Smith, C. R. 1986 Turbulent boundary-layer modification by surface riblets. *AIAA J.* **24**, 1382–1385.

Batchelor, G. K. 1967 *An introduction to fluid dynamics*. Cambridge University Press.

Black, T. J. 1968 An analytical study of the measured wall pressure field under supersonic turbulent boundary layers. NASA CR-888.

Blackwelder, R. F. & Eckelmann, H. 1979 Streamwise vortices associated with the bursting phenomenon. *J. Fluid Mech.* **94**, 577–594.

Blackwelder, R. F. & Haritonidis, J. H. 1983 Scaling of the bursting frequency in turbulent boundary layers. *J. Fluid Mech.* **132**, 87–103.

Blackwelder, R. F. & Kaplan, R. E. 1976 On the wall structure of the turbulent boundary layer. *J. Fluid Mech.* **76**, 89.

Blair, M. F. 1991 Boundary layer transition in accelerating flows with intense freestream turbulence. UTRC-91-1, United Technologies Research Center, Hartford, Connecticut.

PHILOSOPHICAL TRANSACTIONS OF THE ROYAL SOCIETY A MATHEMATICAL, PHYSICAL & ENGINEERING SCIENCES

Bogucz, E. A. & Walker, J. D. A. 1988 The turbulent wake at a sharp trailing edge. *J. Fluid Mech.* **196**, 555–584.

Callegari, A. J. & Ting, L. 1978 Motion of a curved vortex filament with decaying vortical core and axial vleocity. *SIAM J. appl. Math.* **35**, 148–176.

Cerra, A. W. & Smith, C. R. 1983 Experimental observation of vortex ring interaction with fluid adjacent to a surface. Rep. FM-11, Department of Mechanical Engineering and Mechanics, Lehigh University, Bethlehem, Pennsylvania.

Chu, C. C. & Falco, R. E. 1988 Vortex ring/viscous wall layer interaction model of the turbulence production process near walls. *Exp. Fluids* **6**, 305.

Chuang, F. S. & Conlisk, A. T. 1989 Effect of interaction on the boundary layer induced by a convected rectilinear vortex. *J. Fluid Mech.* **200**, 337–365.

Corino, E. R. & Brodkey, R. S. 1969 A visual investigation of the wall region in turbulent flow. *J. Fluid Mech.* **37**, 1–30.

Cowley, S. J., Van Dommelen, L. L. & Lam, S. T. 1991 On the use of lagrangian variables in descriptions of unsteady boundary-layer separation. *Phil. Trans. R. Soc. Lond.* A **333**, 343–378.

Degani, A. T., Smith, F. T. & Walker, J. D. A. 1991 The three-dimensional turbulent boundary layer near a plane of symmetry. *J. Fluid Mech.* (Submitted.)

Doligalski, T. L. & Walker, J. D. A. 1978 Shear layer breakdown due to vortex motion. *Proceedings of AFOSR Workshop on Coherent Structures in Turbulent Boundary Layers* (ed. C. R. Smith & D. E. Abbott), pp. 288–339.

Doligalski, T. L. & Walker, J. D. A. 1984 Boundary layer induced by a convected two-dimensional vortex. *J. Fluid Mech.* **139**, 1–28.

Elliott, J. W., Cowley, S. J. & Smith, F. T. 1983 Breakdown of boundary layers: (i) on moving surfaces; (ii) in self-similar unsteady flow; (iii) in fully unsteady flow. *Geophys. Astrophys. Fluid Dynamics* **25**, 77–138.

Ersoy, S. & Walker, J. D. A. 1985 Viscous flow induced by counter-rotating vortices. *Phys. Fluids* **28**, 2687–2698.

Ersoy, S. & Walker, J. D. A. 1986 Flow induced at a wall by a vortex pair. *AIAA J.* **24**, 1597–1605.

Ersoy, S. & Walker, J. D. A. 1987 The boundary layer due to a three-dimensional vortex loop. *J. Fluid Mech.* **185**, 569–598.

Falco, R. E. 1977 Coherent motions in the outer region of turbulent boundary layers. *Phys. Fluids* **20**, S124–S132.

Falco, R. E. 1981 Structural aspects of turbulence in boundary layer flows. *Proc. 6th Symp. Turbulence* (ed. G. K. Patterson & J. K. Zakin). Department of Chemical Engineering, University of Missouri-Rolla.

Falco, R. E. 1982 A synthesis and model of turbulence structure in the wall region. In *Structure of turbulence in heat and mass transfer* (ed. Z. Zaric), pp. 43–57. Hemisphere.

Falco, R. E. 1991 A coherent structure model of the turbulent boundary layer and its ability to predict Reynolds number dependence. *Phil. Trans. R. Soc. Lond.* A **336**, 103–129. (This volume.)

Frisch, U. & Orzag, S. A. 1990 Turbulence: challenges for theory and experiment. *Physics Today* **43**, 24–32.

Grass, A. J. 1971 Structural feature of turbulent flow over smooth and rough boundaries. *J. Fluid Mech.* **50**, 233–255.

Grass, A. J., Stuart, R. J. & Monsour-Tehrani, M. 1991 Vortical structures and coherent motion in turbulent flow over rough boundaries. *Phil. Trans. R. Soc. Lond.* A **336**, 35–65. (This volume.)

Greco, J. J. & Smith, C. R. 1991 The flow structure in the vicinity of a cylinder–flat plate junction: flow regimes, periodicity, and vortex interactions. Report FM-18, Department of Mechanical Engineering and Mechanics, Lehigh University, Bethlehem, Pennsylvania.

Gretta, W. J. 1990 An experimental study of the fluid mixing effects and flow structure due to a surface mounted passive vortex generating device. M.S. thesis, Department of Mechanical Engineering and Mechanics, Lehigh University, Bethlehem, Pennsylvania.

Haidari, A. H. & Smith, C. R. 1988 Development of the turbulent near-wake of a tapered thick flat plate. *J. Fluid Mech.* **189**, 135–163.

PHILOSOPHICAL TRANSACTIONS OF THE ROYAL SOCIETY A MATHEMATICAL, PHYSICAL & ENGINEERING SCIENCES

Haidari, A. H. & Smith, C. R. 1991 Generation and growth of single hairpin vortices. Report FM-16, Department of Mechanical Engineering and Mechanics, Lehigh University, Bethlehem, Pennsylvania.

Hama, F. R. 1962 Progressive deformation of a curved vortex filament by its own induction. *Phys. Fluids* **5**, 1156–1162.

Hatziavramidis, D. T. & Hanratty, T. J. 1979 The representation of the viscous wall region by a regular eddy pattern. *J. Fluid Mech.* **95**, 655.

Harvey, J. K. & Perry, F. J. 1971 Flowfield produced by trailing vortices in the vicinity of the ground. *AIAA J.* **9**, 1659–1660.

He, J., Kazakia, J. Y. & Walker, J. D. A. 1990 Embedded function methods for supersonic boundary layers. *AIAA Pap.* 90-0306.

Head, M. R. & Bandyopadhyay, P. 1981 New aspects of turbulent boundary layer structure. *J. Fluid Mech.* **107**, 297–338.

Hon, T. L. & Walker, J. D. A. 1987 An analysis of the motion and effects of hairpin vortices. AFOSR Rep. FM-11, Dept Mech. Eng. and Mech., Lehigh University; see also NASA Tech. Memo. 100858, ICOMP-88-9.

Kim, J., Moin, P. & Moser, R. 1987 Turbulence statistics in fully developed channel flow at low Reynolds number. *J. Fluid Mech.* **177**, 133.

Kline, S. J., Reynolds, W. C., Schraub, F. A. & Runstadler, P. W. 1967 The structure of turbulent boundary layers. *J. Fluid Mech.* **95**, 741–773.

Kline, S. J. & Robinson, S. K. 1989 Quasi-coherent structures in the turbulent boundary layer. I. Status report on a community-wide survey of the data. In *Near-Wall Turbulence. Proc. Zaric Meml. Conf.* (ed. S. J. Kline & N. H. Afgan), pp. 200–217. New York: Hemisphere.

Kuchemann, D. 1965 Report on IUTAM symposium on concentrated vortex motion in fluids. *J. Fluid Mech.* **21**, 1–20.

Lighthill, M. J. 1963 In *Laminar boundary layers* (ed. L. Rosenhead), pp. 46–109. Oxford University Press.

Liu, C. H., Krause, E. & Ting, L. 1985 Vortex-dominated flow with viscous core structure. *AIAA Pap.* 85–1556.

Liu, C. H., Tavantzis, J. & Ting, L. 1986 Numerical studies of motion and decay of vortex filaments. *AIAA J.* **24**, 1290–1297.

Lu, L. J. & Smith, C. R. 1985 Image processing of hydrogen bubble flow visualization for determination of turbulence statistics and bursting characteristics. *Exp. Fluids* **3**, 349–356.

Lu, L. J. & Smith, C. R. 1988 Image processing of hydrogen bubble flow visualization for quantitative evaluation of hairpin-type vortices as a flow structure of turbulent boundary layers. Report FM-14, Department of Mechanical Engineering and Mechanics, Lehigh University, Bethlehem, Pennsylvania.

Lu, L. J. & Smith, C. R. 1991 Use of quantitative flow visualization data for examination of spatial-temporal velocity and burst-type characteristics in a turbulent boundary layer. *J. Fluid Mech.* (In the press.)

Milne-Thomson, L. M. 1962 *Theoretical hydrodynamics*. London: Macmillan.

Moin, P. & Kim, J. 1986 The structure of the vorticity field in turbulent channel flow. Part 2. Study of ensemble-averaged fields. *J. Fluid Mech.* **162**, 339–363.

Morkovin, M. V. 1969 Air Force Flight Dynamics Laboratory Report AFFDL-TR-68-149.

Moore, D. W. 1972 Finite amplitude curves on aircraft trailing vortices. *Aero. Q.* **23**, 307–314.

Offen, G. R. & Kline, S. J. 1975 A proposed model of the bursting process in turbulent boundary layers. *J. Fluid Mech.* **70**, 209–228.

Peridier, V. J. & Walker, J. D. A. 1989 Vortex-induced boundary-layer separation. Report FM-13, Department of Mechanical Engineering and Mechanics, Lehigh University; AFOSR-TR-90-0458 (available as ADA-221564).

Peridier, V. J., Smith, F. T. & Walker, J. D. A. 1991*a* Vortex-induced boundary-layer separation. Part I. The limit problem $Re \to \infty$. *J. Fluid Mech.* (In the press.)

Peridier, V. J., Smith, F. T. & Walker, J. D. A. 1991*b* Vortex-induced boundary-layer separation. Part II. Unsteady interacting boundary-layer theory. *J. Fluid Mech.* (In the press.)

PHILOSOPHICAL TRANSACTIONS OF THE ROYAL SOCIETY A MATHEMATICAL, PHYSICAL & ENGINEERING SCIENCES

Perry, A. E. & Chong, M. S. 1982 On the mechanism of wall turbulence. *J. Fluid Mech.* **119**, 173–217.

Robinson, S. K. 1990 A perspective on coherent structures and conceptual models for turbulent boundary layer physics. *AIAA Pap.* no. 90-1638.

Robinson, S. K. 1991 Coherent motions in the turbulent boundary layer. *A. Rev. Fluid Mech.* **23**, 601–639.

Robinson, S. K. & Kline, S. J. 1990 Turbulent boundary layer structure: progress, status and challenges. In *Structure of turbulence and drag reduction* (ed. A. Gyr), pp. 3–22. Springer-Verlag.

Sears, W. P. & Telionis, D. P. 1975 Boundary-layer separation in unsteady flow. *SIAM J. appl. Math.* **28**, 215–235.

Smith, C. R. 1984 A synthesized model of the near-wall behavior in turbulent boundary layers. *Proceedings of 8th Biennial Symposium on Turbulence* (ed. J. L. Zakin & G. Patterson), p. 35. University of Missouri-Rolla.

Smith, C. R. & Lu, L. J. 1990 The use of a template matching technique to identify hairpin vortex flow structures in turbulent boundary layers. *Proceedings of Zaric International Seminar on Wall Turbulence* (ed. S. J. Kline). Hemisphere.

Smith, C. R. & Metzler, S. P. 1983 The characteristics of low-speed streaks in the near-wall region of a turbulent boundary layer. *J. Fluid Mech.* **129**, 27–54.

Smith, C. R., Walker, J. D. A., Haidari, A. H. & Taylor, B. K. 1990 Hairpin vortices in turbulent boundary layers; the implications for reducing surface drag. In *Structure of turbulence and drag reduction* (ed. A. Gyr), pp. 51–58. Springer-Verlag.

Smith, F. T. 1988 Finite-time breakup can occur in any unsteady interacting boundary layer. *Mathematika* **35**, 256–273.

Sobrun, U. 1991 Ph.D. thesis, Lehigh University. (In preparation.)

Spalart, P. R. 1988 Direct simulation of a turbulent boundary layer up to $Re_\theta = 1410$. *J. Fluid Mech.* **187**, 61–98.

Taylor, B. & Smith, C. R. 1990 Pressure gradient effects on the development of hairpin vortices in an initially laminar boundary layer. Report FM-15, Department of Mechanical Engineering and Mechanics, Lehigh University, Bethlehem, Pennsylvania.

Theodorsen, T. 1952 Mechanism of turbulence. *Proceedings Second Midwestern Conference on Fluid Mechanics*, *Bull.* no. 149. Ohio State University, Columbus, Ohio.

Uzkan, T. & Reynolds, W. C. 1967 A turbulent boundary layer on a wall moving at the free-stream velocity. *J. Fluid Mech.* **28**, 803.

Van Dommelen, L. L. 1981 Unsteady boundary-layer separation. Ph.D dissertation, Cornell University.

Van Dommelen, L. L. & Cowley, S. J. 1990 On the lagrangian description of unsteady boundary-layer separation. Part 1. General theory. *J. Fluid Mech.* **210**, 593–626.

Van Dommelen, L. L. & Shen, S. F. 1980 The spontaneous generation of the singularity in a separating boundary layer. *J. Comp. Phys.* **38**, 125–140.

Van Dommelen, L. L. & Shen, S. F. 1982 The genesis of separation. *Proc. Symp. Numerical and Physical Aspects of Aerodynamic Flow* (ed. T. Cebeci), pp. 283–311. Long Beach, California.

Walker, J. D. A. 1978 The boundary layer due to rectilinear vortex. *Proc. R. Soc. Lond.* A **359**, 167–188.

Walker, J. D. A. 1990*a* Wall-layer eruptions in turbulent flows. *2nd IUTAM Symp. Structure of Turbulence and Drag Reduction* (ed. A. Gry). Springer-Verlag; also NASA Tech. Memo. 102362, ICOMP-89-26.

Walker, J. D. A. 1990*b* Models based on dynamical features of the wall layer. *Appl. Mech. Rev.* **43**, S232–S239.

Walker, J. D. A., Abbott, D. E., Sharnhorst, R. K. & Weigand, G. G. 1989 Wall-layer model for velocity profile in turbulent flows. *AIAA J.* **27**, 140–149.

Walker, J. D. A., Ece, M. C. & Werle, M. J. 1991 An embedded function approach for turbulent flow prediction. *AIAA J.* (In the press.)

Walker, J. D. A. & Herzog, S. 1988 Eruption mechanisms for turbulent flow near walls. In *Transport phenomena in turbulent flows* (ed. M. Hirata & N. Kasagi), pp. 145–156. Hemisphere.

PHILOSOPHICAL TRANSACTIONS OF THE ROYAL SOCIETY A MATHEMATICAL, PHYSICAL & ENGINEERING SCIENCES

Walker, J. D. A., Smith, C. R., Doligalski, T. L. & Cerra, A. W. 1987 Impact of a vortex ring on a wall. *J. Fluid Mech.* **181**, 99–140.

Wallace, J. M. 1982 On the structure of bounded turbulent shear flow. A personal view. In *Developments in theoretical and applied mechanics, XI* (ed. T. J. Chung & G. R. Karr), p. 509. Department of Mechanical Engineering, University of Huntsville, Huntsville, Alabama.

Wallace, J. M. & Balint, J. L. 1987 Viscous drag reduction using streamwise aligned riblets: survey and new results. *Turbulence management and relaminarization* (ed. H. W. Liepman & R. Narashima), p. 134. Hemisphere.

Wallace, J. M. & Balint, J. L. 1990 Flow visualization study of the effects of trip type on the structure of the turbulent boundary layer. Video Tape, Turbulence Laboratory, University of Maryland.

Wallace, J. M., Eckelman, H. & Brodkey, R. S. 1972 The wall region of turbulent shear flow. *J. Fluid Mech.* **54**, 39–48.

Willmarth, W. W. 1975 Structure of turbulence in boundary layers. *Adv. appl. Mech.* **15**, 159–254.

Willmarth, W. W. & Lu, S. S. 1972 Structure of the Reynolds stress near the wall. *J. Fluid Mech.* **55**, 65–92.

Willmarth, W. W. & Tu, B. J. 1967 Structure of turbulence in the boundary layer near a wall. *Phys. Fluids* **10**, S134.

Zang, T. A. 1991 Numerical simulation of the dynamics of turbulent boundary layers: perspectives of a transition simulator. *Phil. Trans. R. Soc. Lond.* A **336**, 95–102. (This volume.)

PHILOSOPHICAL TRANSACTIONS OF THE ROYAL SOCIETY A MATHEMATICAL, PHYSICAL & ENGINEERING SCIENCES

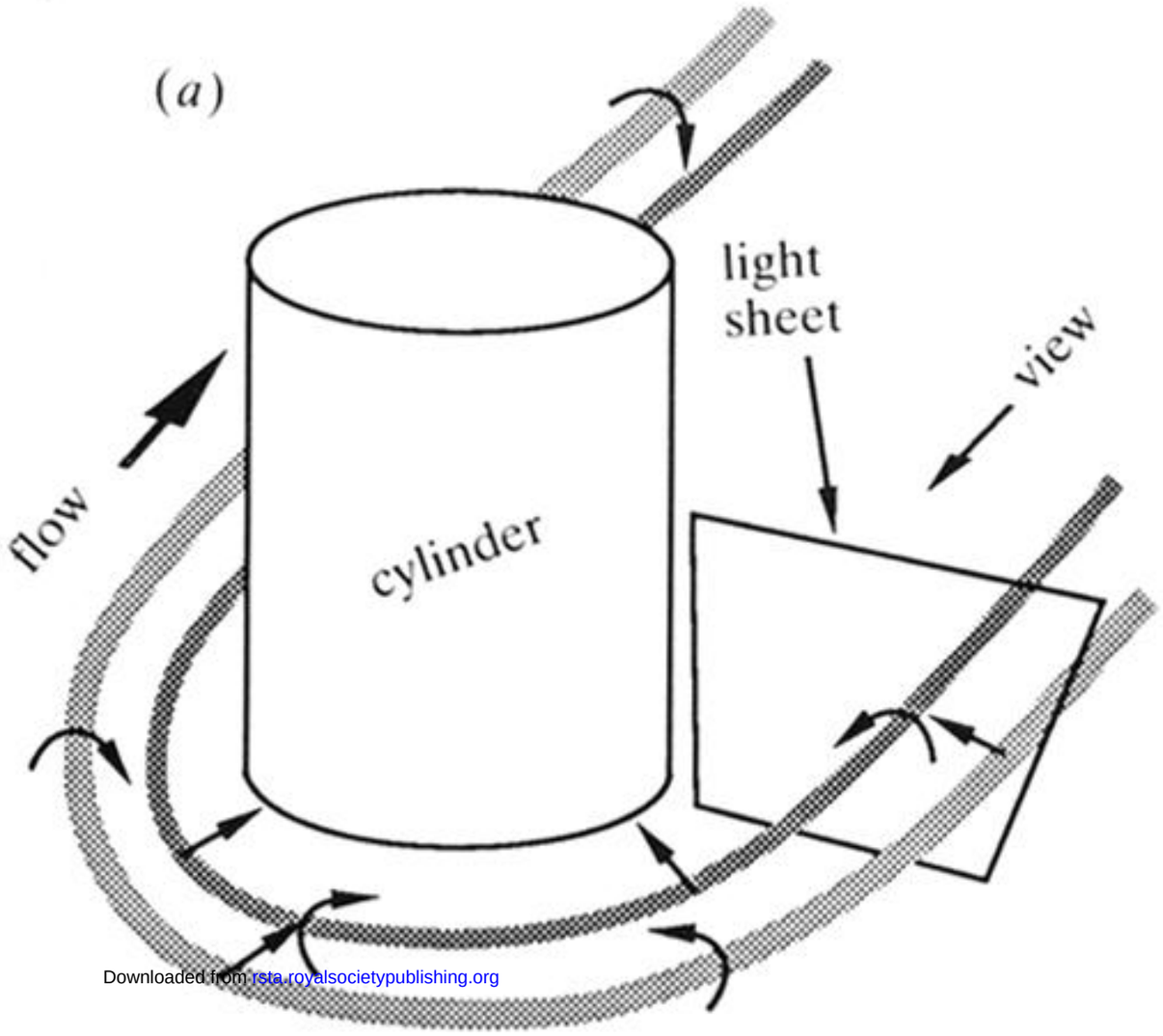

Figure 5. End-view of necklace vortex legs and induced surface eruptions. Visualization using hydrogen bubbles and light-sheet illumination. (*c*)–(*f*) A temporal sequence of end-view photographs illustrating streamwise necklace vortex legs and associated surface eruptions.

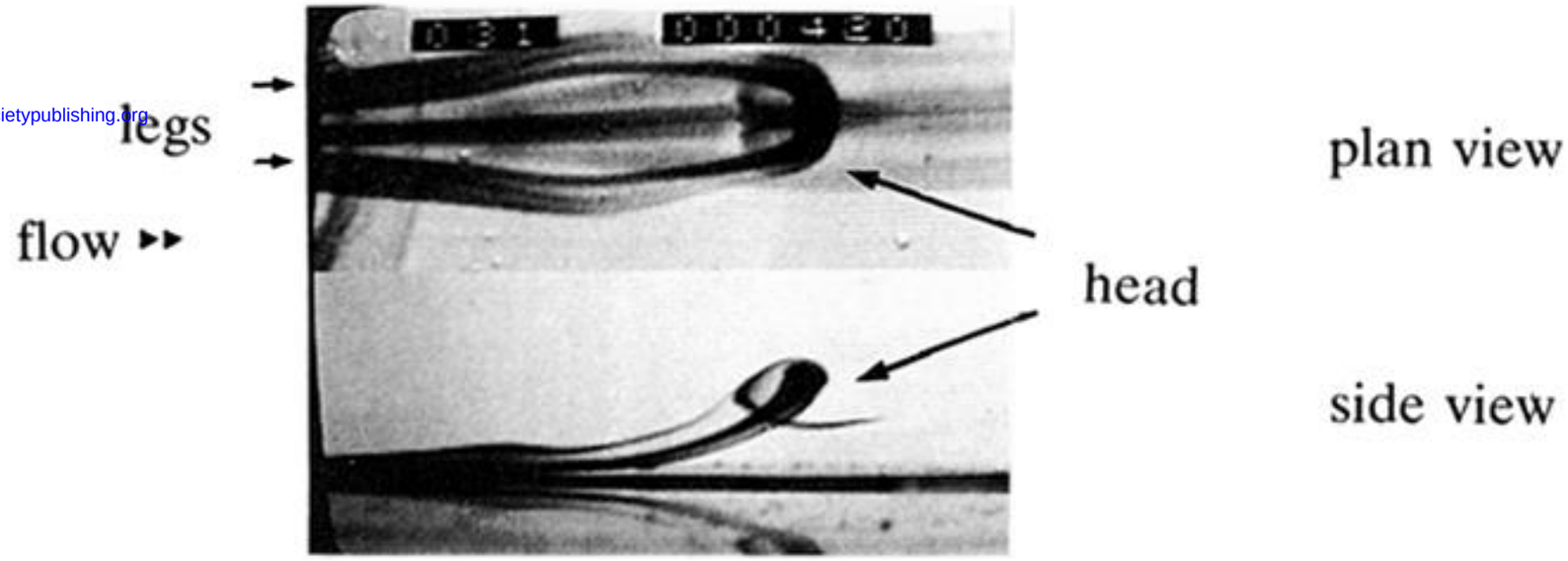

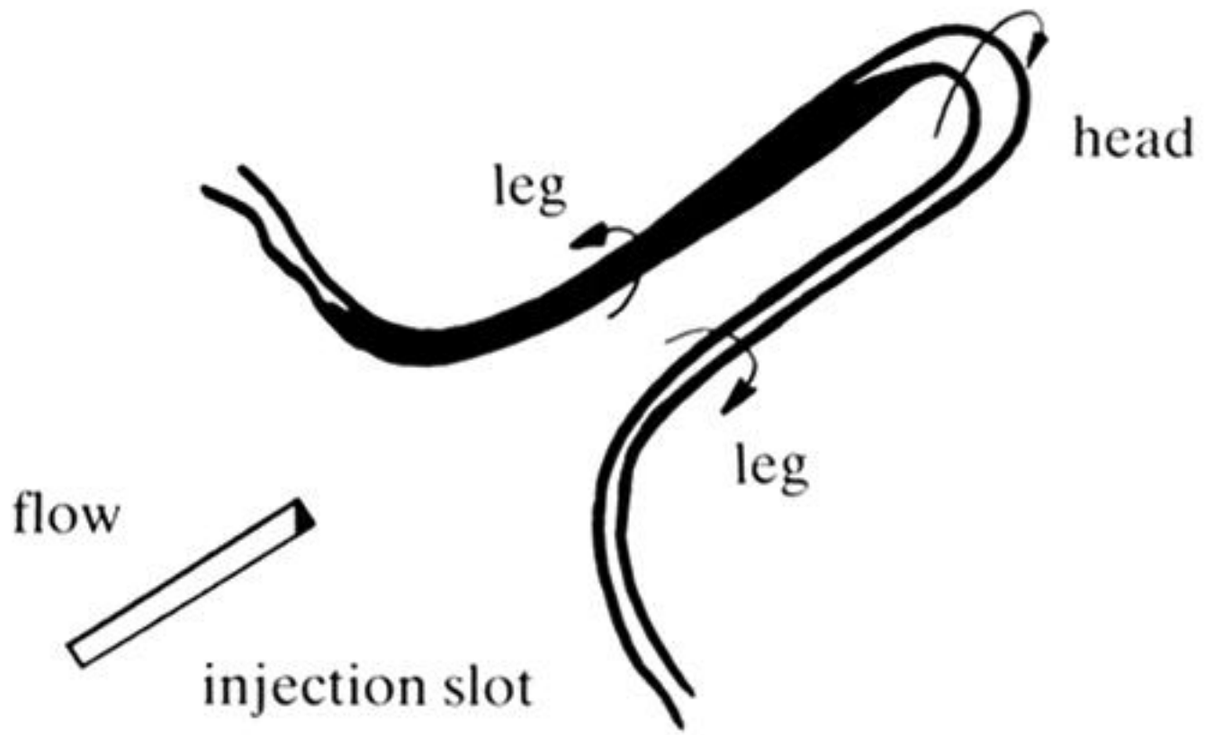

igure 15. Illustration of experimental generation of a single hairpin vortex by surface injection sing system shown in figure 14. (*a*) Dual-view picture of dye-marked single hairpin vortex. (*b*) ometric schematic of single hairpin after generation.

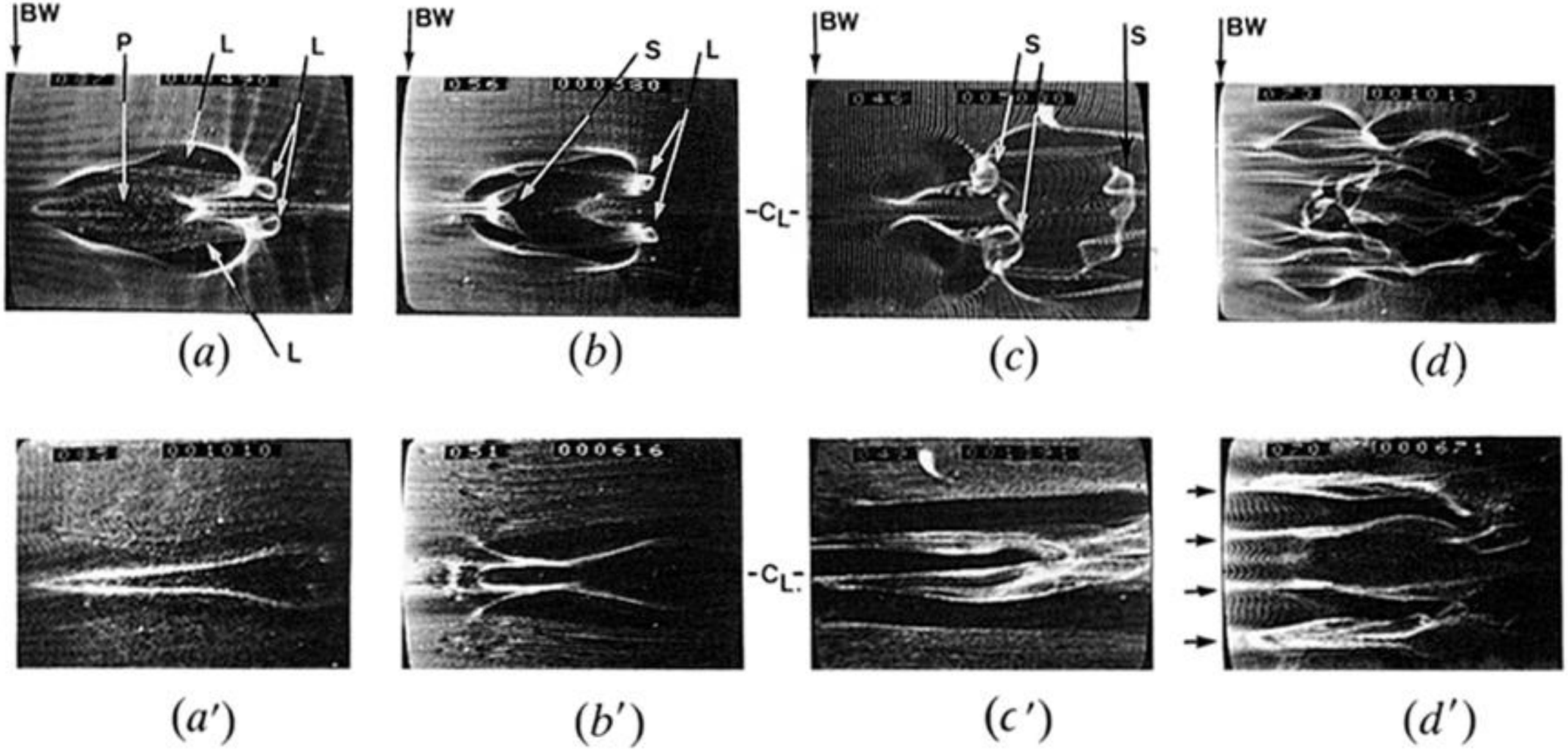

Figure 17. Dual-level, plan view visualization of hydrogen bubble patterns generated by left-to-right passage of developing hairpin vortex (cf. figure 16). BW denotes the position of the bubble wire, P the location of an initial 'pocket' formation (Falco 1991), L the location of the vortex legs, S the evolution of secondary hairpin vortices (see §5), and C_L the plane of symmetry. Bubbles are generated at $y/\delta = 0.4$ for upper row visualizations and $y/\delta = 0.1$ for lower row visualizations.

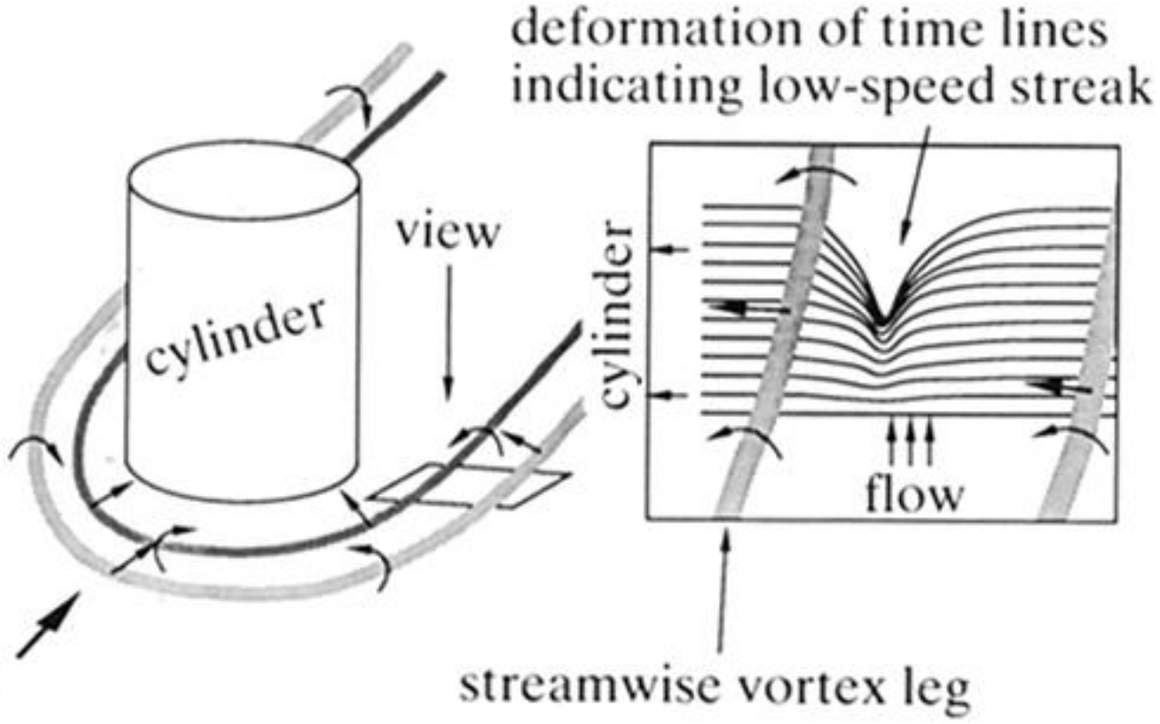

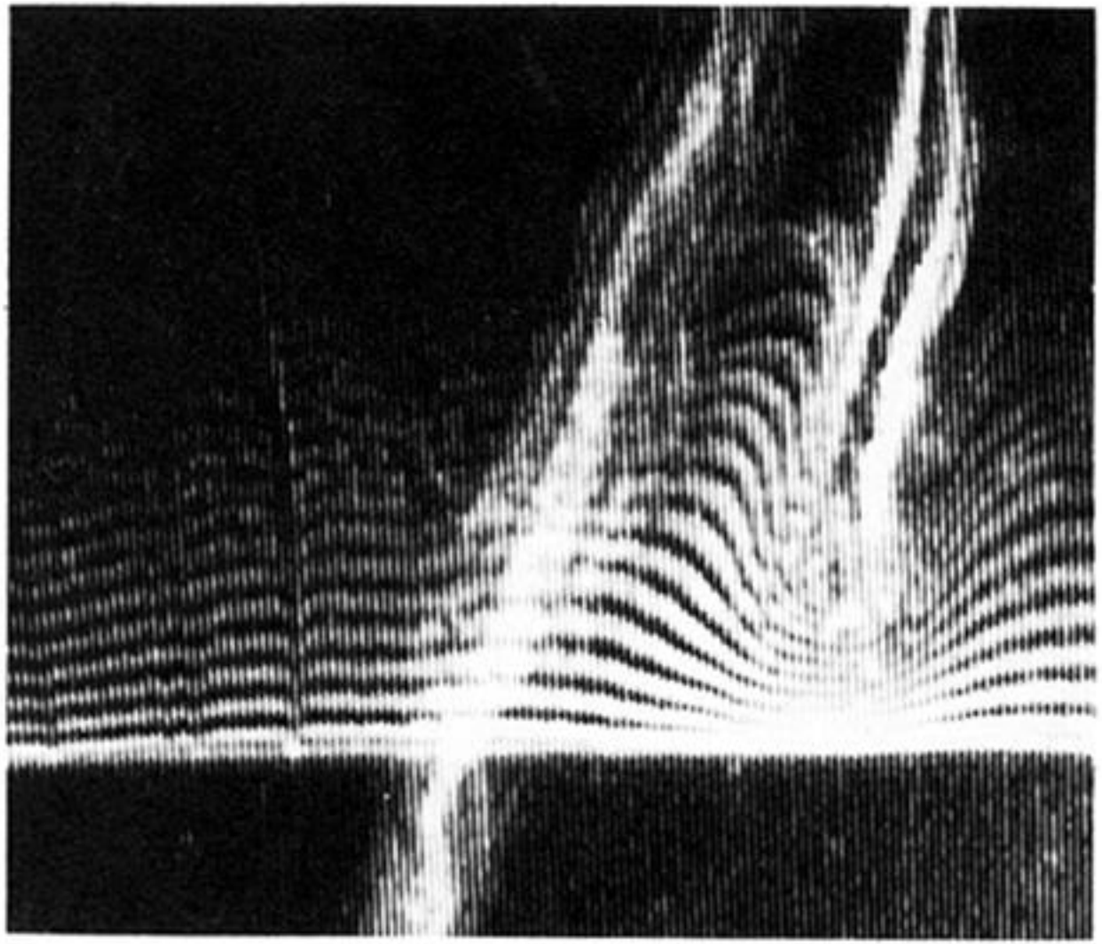

Figure 18. Plan-view of necklace vortex leg interaction to create low-speed streak. Plan-view photograph shows a streamwise necklace vortex leg (visualized by upstream hydrogen bubble wire) interacting with surface fluid (visualized by bubble wire near surface) to create low-speed streak at surface.

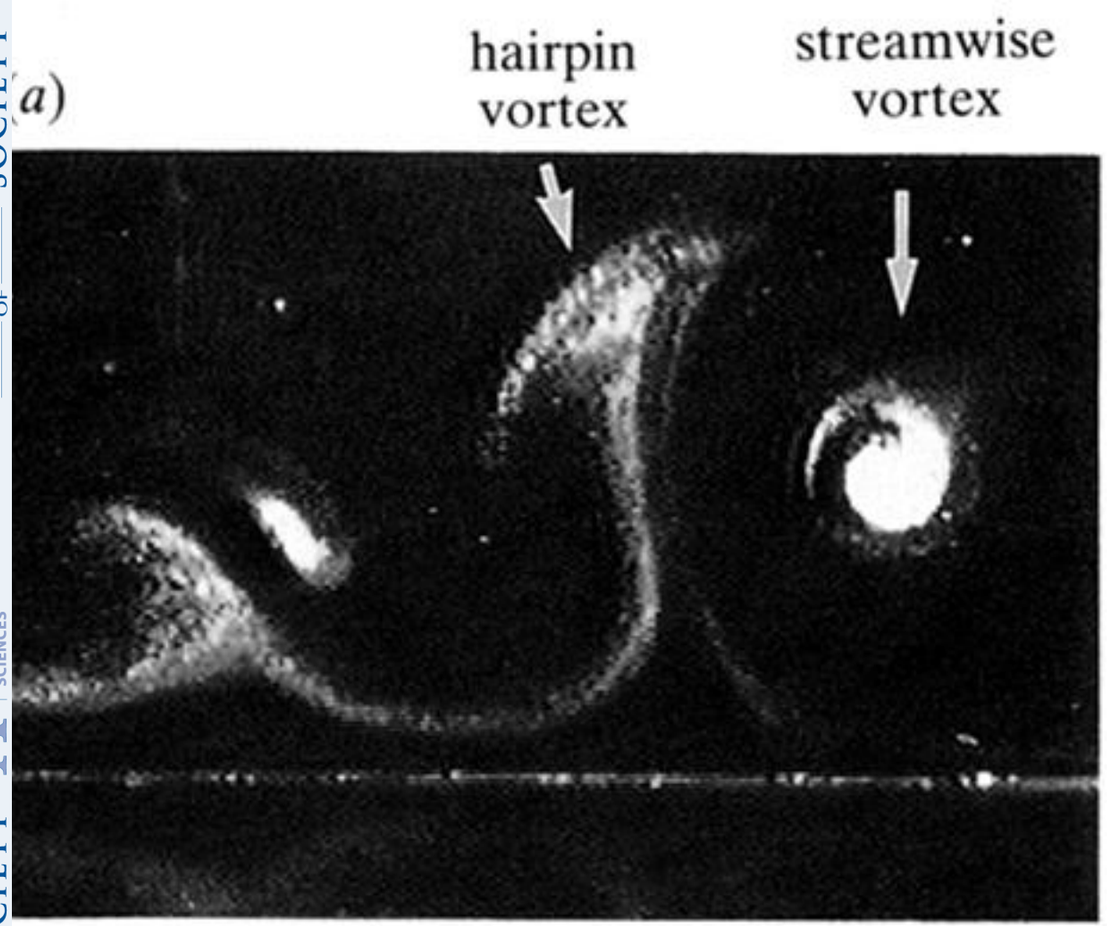

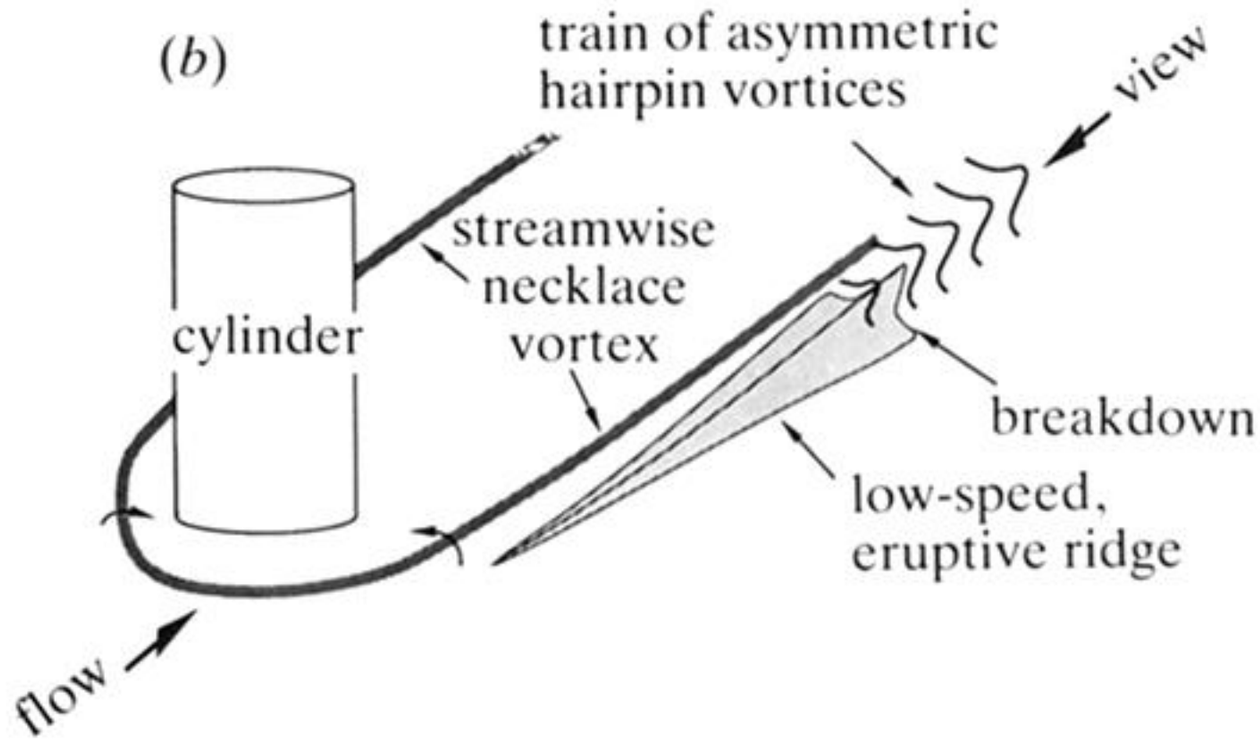

igure 20. Characteristics of the breakdown of the eruptive spires induced by streamwise necklace ortex legs. (*a*) End-view, light-sheet photograph showing the breakdown of an eruptive spire (low-peed ridge) induced by a streamwise necklace vortex leg. (*b*) Schematic illustrating the general reakdown process for the low-speed, eruptive ridge.

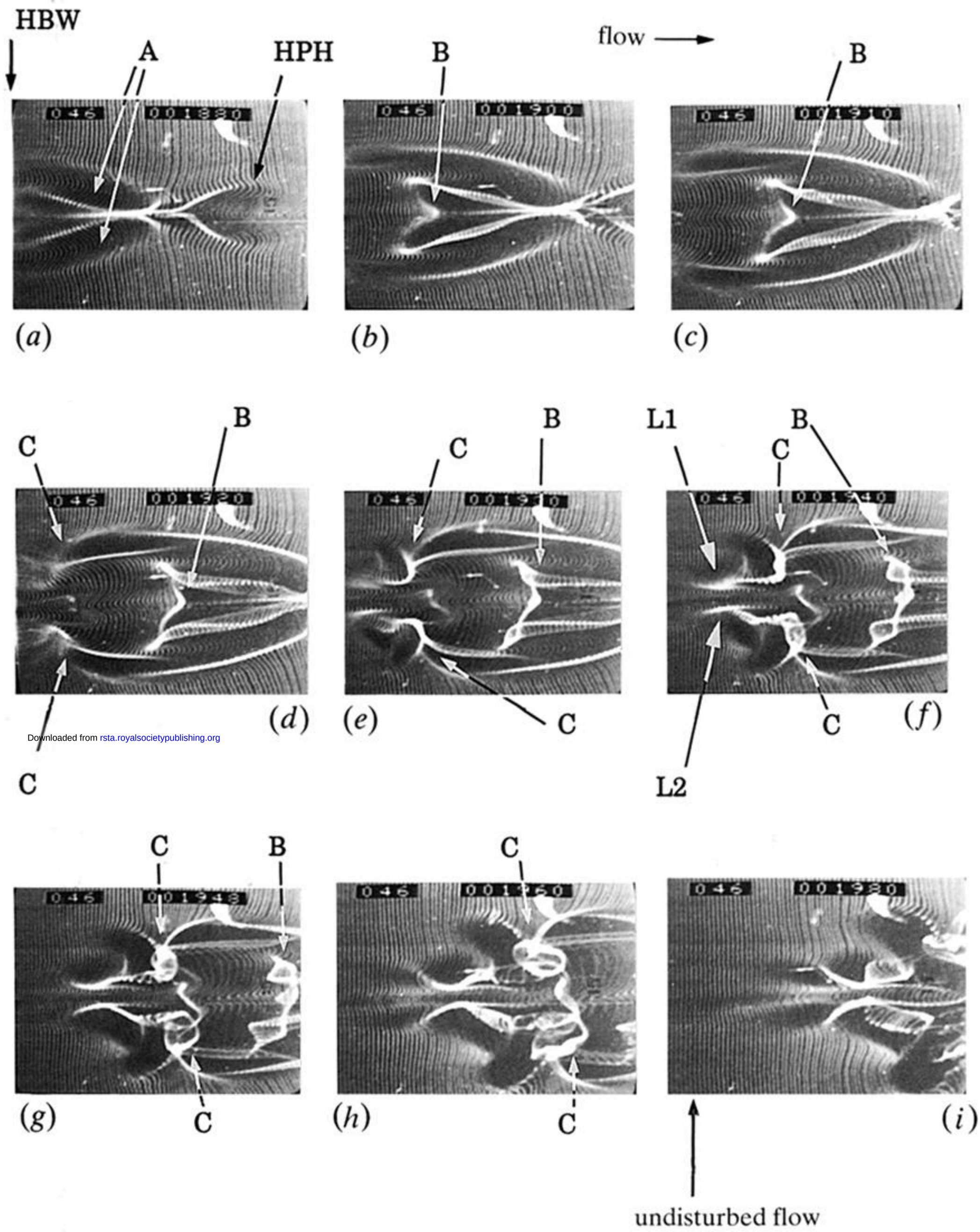

Figure 23. Plan-view hydrogen bubble wire visualization sequence illustrating the development of secondary vortices near the surface as a primary hairpin vortex passes a fixed streamwise location. HBW denotes the position of the hydrogen bubble wire, HPH is the location of head of primary vortex, A the location of the trailing legs of primary vortex, B the development of a secondary vortex behind head of primary, C the development of secondary vortices adjacent to the legs of the primary vortex, and L1, L2 the legs nearest the symmetry plane for the secondary vortices indicated by C. (*a*) $t = 0$ s; (*b*) $t = 0.166$ s; (*c*) $t = 0.25$ s; (*d*) $t = 0.33$ s; (*e*) $t = 0.146$ s; (*f*) $t = 0.5$ s; (*g*) $t = 0.58$ s; (*h*) $t = 0.666$ s; (*i*) $t = 0.833$ s.

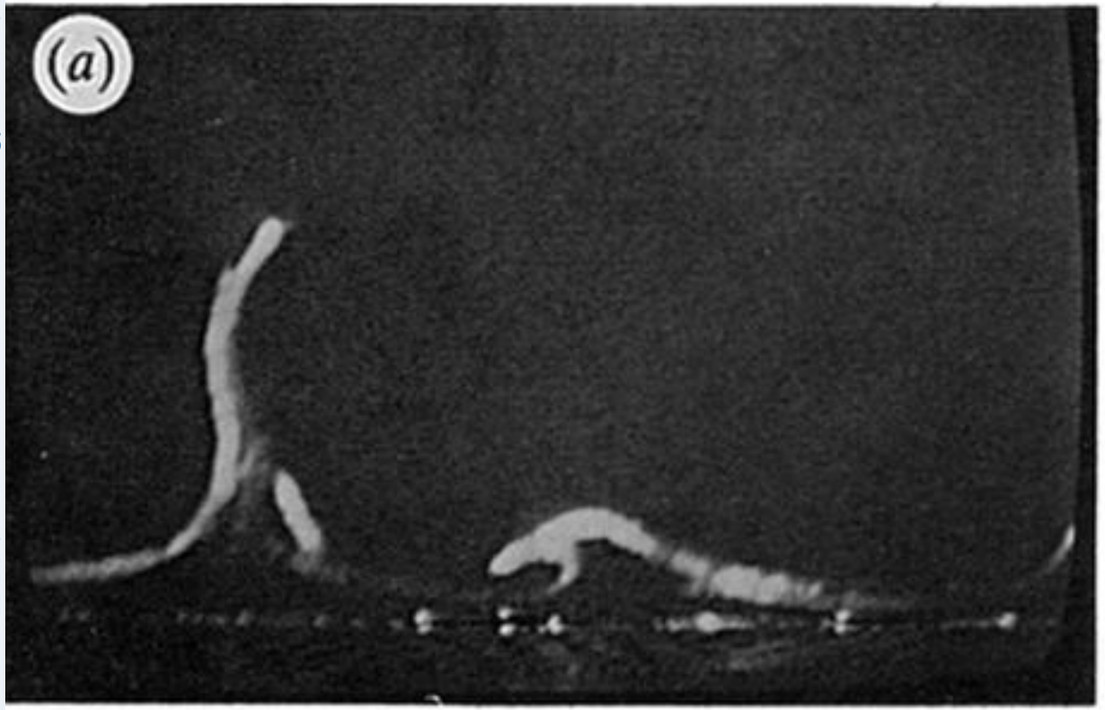

Figure 26. End-view visualization, using a horizontal hydrogen bubble wire and laser light-sheet illumination (see figure 25), showing eruptive spires emanating from near-wall region of a turbulent boundary layer ($Re_\theta \approx 1150$). Lateral vield of view *ca.* 250 wall units, wire located $y^+ = 7$ from surface, and $x^+ \approx 150$ upstream of light sheet. Compare with eruptions induced by streamwise vortex as shown in figure 5. Tip penetration: (*a*) $y^+ = 92$; (*b*) $y^+ = 105$.